Exelon Generation

NP-11-0028
June 30, 2011

10 CFR 52, Subpart A

U.S. Nuclear Regulatory Commission
ATTN: Document Control Desk
Washington, DC 20555-0001

Subject: Exelon Nuclear Texas Holdings, LLC
Victoria County Station Early Site Permit Application
Response to Request for Additional Information Letter No. 07
NRC Docket No. 52-042

Attached are responses to NRC staff questions included in Request for Additional Information (RAI) Letter No. 07, dated April 8, 2011, related to Early Site Permit Application (ESPA), Part 2, Sections 02.04.06, 02.05.02, and 11.02. NRC RAI Letter No. 07 contained twenty Questions. This submittal comprises a partial response to RAI Letter No. 07, and includes responses to the following two (2) Questions:

02.04.06-3 02.05.02-10

When a change to the ESPA is indicated by a Question response, the change will be incorporated into the next routine revision of the ESPA, planned for no later than March 31, 2012.

Of the remaining eighteen (18) RAIs associated with RAI Letter No. 07, responses to seven (7) Questions were submitted to the NRC in Exelon Letter NP-11-0016, dated May 5, 2011, responses to seven (7) Questions were submitted to the NRC in Exelon Letter NP-11-0020, dated May 23, 2011, and response to one (1) Question was submitted to the NRC in Exelon Letter NP-11-0025, dated June 17, 2011. The response to RAI Questions 02.05.02-3a, 02.05.02-3b, and 02.05.02-3c will be provided by August 5, 2011. These response times are consistent with the response times described in NRC RAI Letter No. 07, dated April 8, 2011.

Regulatory commitments established in this submittal are identified in Attachment 3. If any additional information is needed, please contact David J. Distel at (610) 765-5517.

I declare under penalty of perjury that the foregoing is true and correct. Executed on the 30th day of June, 2011.

Respectfully,

Marilyn C. Kray
Vice President, Nuclear Project Development

Attachments:
1. Question 02.04.06-3
2. Question 02.05.02-10
3. Summary of Regulatory Commitments

cc: USNRC, Director, Office of New Reactors/NRLPO (w/Attachments)
USNRC, Project Manager, VCS, Division of New Reactor Licensing (w/Attachments)
USNRC Region IV, Regional Administrator (w/Attachments)

RAI 02.04.06-3:

Question:

To meet the requirements of GDC 2, 10 CFR 52.17, and 10 CFR Part 100, an assessment of the Probable Maximum Tsunami (PMT) for the proposed site should be provided in the application. Section C.I.2.4.6.4 of Regulatory Guide 1.206 (RG 1.206) provides specific guidance with respect to tsunami analysis. This includes providing a complete description of the analysis procedure used to calculate tsunami wave height and period at the site, including the theoretical bases of the models, their verification and the conservatism of all input parameters. Specifically, for this site, the applicant should provide in the SSAR a quantitative analysis regarding:

(1) Choice of the East Breaks slide as the PMT source over other potential sources.

Section C.I.2.4.6.3 of RG 1.206 provides specific guidance with respect to the source characteristics needed to determine the PMT. These characteristics include detailed geo-seismic descriptions of the controlling local and distant tsunami generators, including location, source dimensions, fault orientation, and maximum displacement. Provide these characteristics for seismogenic tsunamis originating in the Caribbean and Gulf of Mexico as used in the analysis. Also provide the location, source volume and dimensions, and maximum displacement information for landslides in the Gulf of Mexico used in the analysis. In addition, provide a rationale for choosing the East Breaks slide as the PMT source among other potential sources based on analysis of estimated tsunami water levels at the VCS site for each source.

(2) Propagation of the PMT from the source to the site, using bathymetric, coastline, and topographic information specific to the site.

Section C.I.2.4.6.4 of RG 1.206 provides specific guidance with respect to tsunami analysis. This includes providing a complete description of the analysis procedure used to calculate tsunami wave height and period specific to the bathymetry and topography between the PMT source and the VCS site. Provide a clear presentation of all equations used, discussion of assumptions inherent in these equations and the associated conservatism, and the procedure to calculate the provided values. In addition, provide all input data sources, calculation packages, and any associated modeling input files.

Response:

The response to RAI 02.04.06-3 is provided in three sections. The first section provides general information for the Exelon VCS site. The second section provides a response to Item (1) of RAI 02.04.06-3. The third section provides a response to Item (2) of RAI 02.04.06-3. Some items in this response were also addressed in the response to RAI 02.04.06-1 (Reference 1). These items are noted in the response.

General Information:

As stated in Section 2.4.1.1 of the VCS Early Site Permit (ESP), VCS is located in Victoria County, Texas near the west bank of the Guadalupe River, at River Mile 29.6 (proposed SSAR Figure 2.4.6-8, attached). VCS is approximately 13 miles south of the

city of Victoria, Texas, and 8 miles west of Bloomington, Texas, near U.S. Highway 77, and 36 miles inland from the nearest point of Texas Gulf Coast shoreline. The VCS site consists primarily of the power block area, which includes all safety-related facilities, and approximately 4900 acres for a nonsafety-related cooling basin. The minimum finished site grade elevation for the power block is 95.0 feet in North American Vertical Datum of 1988 (NAVD 88).

Response Item (1):

Responses to Item (1) are provided in three parts, each of which addresses a specific part of Item (1). The part of Item (1) addressed in each part of this response is cited again before the response. Part (a) discusses source generator characteristics for SSAR Subsection 2.4.6.3, including seismogenic tsunamis, seismic seiches, and volcanoes. Part (b) discusses the location, source volume and dimensions, and maximum displacement information for submarine mass failures (SMFs), which includes submarine landslides and submarine slumps, in the Gulf of Mexico. Part (c) provides a rationale for choosing the East Breaks slide as the PMT source.

Part (a)

Section C.I.2.4.6.3 of RG 1.206 provides specific guidance with respect to the source characteristics needed to determine the PMT. These characteristics include detailed geo-seismic descriptions of the controlling local and distant tsunami generators, including location, source dimensions, fault orientation, and maximum displacement. Provide these characteristics for seismogenic tsunamis originating in the Caribbean and Gulf of Mexico as used in the analysis.

Seismogenic Tsunamis: As stated in Reference 2 and Reference 3, seismogenic tsunamis generated outside or within the Gulf of Mexico are not expected to pose a flooding risk to the South Texas coast. Reference 3 states that "tsunami propagation from significant earthquake sources outside the Gulf of Mexico, such as the northern Panama Convergence Zone, Northern South America, Cayman Trough, the Puerto Rico trench, or the Gibraltar area shows that wave amplitude is greatly attenuated by the narrow and shallow passages into the gulf, and as a result, these tsunami sources do not constitute a tsunami hazard to the Gulf of Mexico coast." Detailed seismic source generator characteristics, including potential source zones in the North Panama Deformation Belt and the Northern South American Convergent Zone, are provided in the proposed text markup for SSAR Subsection 2.4.6.3.1. Potential seismogenic tsunamis originating in the Gulf of Mexico and Caribbean were also discussed in the response to Item (2) and Item (3) in RAI 02.04.06-1, respectively (Reference 1).

Seismic Seiches: As discussed in SSAR Subsection 2.4.6.2, the only documented seismic seiche event on the South Texas coast resulted from the March 27, 1964, Gulf of Alaska earthquake. The moment magnitude (M_w) for the March 27, 1964, Gulf of Alaska earthquake was 9.2, which is the second largest earthquake in the historical data record.

The May 22, 1960, earthquake in Chile (M_w=9.5) has the largest moment magnitude in the historical data record. While this earthquake might also have been expected to have caused seiches along the Texas coast, tide gauges along the Gulf Coast did not record any such event. However, a small seiche was observed in Lake Pontchartrain, Louisiana, following the February 27, 2010, Chile (M_w=8.8) earthquake.

Similarly, the February 7, 1812, New Madrid earthquake (M_w=7.8), which is the largest earthquake recorded in the contiguous United States, produced significant seiches in the Mississippi River and in waterways along the Texas state boundary (SSAR Reference

2.4.6-10). However, no records exist to indicate that the 1812 New Madrid earthquake affected the South Texas coast or the Guadalupe River near VCS.

In summary, Reference 3 states that "it is likely that seismic seiche waves resulting from the 1964 Gulf of Alaska earthquake are nearly the highest that can be generated owing to a predominantly continental ray path for seismic surface waves from Alaska to the Gulf Coast."

Volcanogenic Tsunamis: Reference 2 states that a tsunami hazard does not exist for the US Gulf Coast from volcanism. Previous studies have stated that the eruption and collapse of the Cumbre Vieja volcano on the island of La Palma in the Canary Islands could potentially affect the coast of Florida with a 25 m wave (SSAR Reference 2.4.6-7). An assessment of the SSAR Reference 2.4.6-7 estimate is provided by Reference 2:

> "as envisioned by Ward and Day (2001) [SSAR Reference 2.4.6-7], a flank collapse of the volcano may drop a rock volume of up to 500 km^3 into the surrounding ocean. The ensuing submarine slide, which was assumed to propagate at a speed of 100 m/s, will generate a strong tsunami with amplitudes of 25 m in Florida. In addition, they claimed that the collapse of Cumbre Vieja is imminent. In our opinion, the danger to the U.S. Atlantic coast from the possible collapse of Cumbre Vieja is exaggerated."

Further research on the La Palma event indicated that the distribution of slide blocks on the ocean bottom suggests that the collapse of Cumbre Vieja may not have been the result of a single catastrophic event, but the result of several smaller events. A recent report on potential tsunami threats to the United Kingdom concluded that "studies of the offshore turbidites [i.e., poorly sorted sediment that is deposited from a density flow of mixed water and sediment] created by landslides from the flanks of the Canary Islands suggest that these result from multiple landslides spread over periods of several days" and are therefore "likely to create tsunamis of only local concern" (Reference 4).

Volcanoes in the Gulf of Mexico were discussed in the response to Item (4) in RAI 02.04.06-1 (Reference 1). The National Geophysical Data Center (NGDC) natural hazard database for volcanoes lists only two volcanoes (Los Atlixcos and San Martin) within 16 km (10 mi) of the present day Gulf of Mexico shoreline. Both volcanoes are located near Veracruz, Mexico. Los Atlixcos is located about 9 km (5.6 mi) from the shoreline and about 975 km (606 mi) from the VCS site. San Martin is located about 13 km (8.0 mi) from the shoreline and about 1127 km (700 mi) from the VCS site. Based on the distance to the shoreline and proximity to VCS, volcanogenic sources near Veracruz, Mexico are not expected to pose a flooding hazard to safety-related functions of VCS.

As no tsunamis have been documented in the Gulf of Mexico as a result of recent volcanic eruptions or associated mass wasting events (gravity-driven mass movement of soil, regolith, or rock moving downslope), this mechanism is not considered as a potential source of tsunamis along the South Texas coast.

Part (b)

Also provide the location, source volume and dimensions, and maximum displacement information for landslides in the Gulf of Mexico used for the analysis.

Reference 2 and Reference 3 cite four credible SMF source areas in the Gulf of Mexico: the Florida Escarpment, Campeche Escarpment, the Northwest Gulf of Mexico, and the Mississippi Canyon (SSAR Figure 2.4.6-1). These four SMF source areas are located in three geologic provinces: a carbonate province (Florida Escarpment and Campeche Escarpment), a salt province (Northwest Gulf of Mexico, including the East Breaks

slump), and a canyon to deep-sea fan province (Mississippi Canyon). The location, source volume and dimensions, and maximum displacement information for maximum credible single events in each region are provided in Reference 2, Reference 3, and Reference 5. Reference 5 estimated a maximum credible single event volume of 16 km^3 and an excavation depth of 150 m for the Florida Escarpment. The runout distance for this source is unknown since the base of the Florida Escarpment is buried under younger Mississippi Fan deposits (SSAR Figure 2.4.6-1) (Reference 2). Similarly, for the East Breaks slump, Reference 3 estimated a maximum credible single event volume of 22 km^3 and an excavation depth of 160 m (shelf to base of headwall scarp). The runout distance was estimated as 130 km from the headwall scarp (Reference 3). Also, as discussed in the response to Item (6) of RAI 02.04.06-1 (Reference 1), source parameters for the East Breaks slump that were used for Method of Splitting Tsunami (MOST) hydrodynamic simulations were estimated independently from three-arc-second bathymetry data from the National Geophysical Data Center (NGDC). For the Mississippi Canyon, Reference 5 estimated a maximum credible single event volume of 426 km^3 and an excavation depth of 300 m. The runout distance was estimated as 442 km from the headwall scarp (Reference 3).

Part (c)

In addition, provide a rationale for choosing the East Breaks slide as the PMT source among other potential sources based on analysis of estimated tsunami water levels at the VCS site for each source.

The East Breaks slump was selected as the PMT source based on its proximity, dimensions and orientation relative to VCS. Also, as discussed in the response to Item (2), hydrodynamic simulations for the East Breaks slump were based on a range of conservative source parameters for the slump dimensions, with a large range in the simulated initial wave dimensions (Table 1). For example, initial wave trough elevations for MOST simulations varied from -7 m to -140 m (-23 ft to -459 ft, respectively) (MSL) (Table 1) (see attached proposed SSAR Figures 2.4.6-13, 2.4.6-14, 2.4.6-15, and 2.4.6-16). Initial wave crest elevations varied from 3 m to 60 m (9.8 ft to 197 ft, respectively) (MSL). Initial wave widths varied from 14 km (8.7 mi) to 136 km (85 mi). Initial deformation areas (i.e., horizontal area of sea surface deformation from 0 ft MSL due to the initial wave) range from about 387 km^2 to about 9,932 km^2 (149 mi^2 to 3835 mi^2, respectively).

SMF sources located in Mississippi Canyon and Florida Margin are not expected to represent the limiting source mechanism for the PMT for the VCS site due to the orientation and much longer distance of these sources relative to VCS (Reference 3). However, Reference 3 states that the Campeche Escarpment, which is 700 km from the East Breaks slump, has equal tsunami impact potential on the Texas coast as the East Breaks slump. Results of independent simulations that were performed for sources at the East Breaks slump and the Campeche Escarpment for Reference 3 are discussed in the response to Item (2).

Response Item (2)

The response to Item (2) is provided in three sections. Part (a) discusses PMT estimates based on Method of Splitting Tsunami (MOST) simulations for a potential source at the East Breaks slump. Part (b) discusses PMT estimates based on independent COULWAVE simulations performed for Reference 3 for potential sources at the East Breaks slump and the Campeche Escarpment. Part (c) discusses the PMT estimate from the MOST simulations relative to the minimum finished grade elevation of the power block.

For all model simulations, initial wave elevations are relative to a still water level of 0 m (0 ft) MSL.

Part (a)

MOST Simulations for the East Breaks slump

Hydrodynamic modeling was performed for a submarine mass failure (SMF) originating at the East Breaks slump for FSAR Subsection 2.4S.6 for the South Texas Project Units 3 & 4 COLA (Reference 6). Hydrodynamic simulations were performed using a series of codes known as MOST (Reference 7 and Reference 8), which has been subject to extensive validation testing (Reference 9 and Reference 10).

MOST is based on three stages of long wave evolution:

Stage 1: A "Deformation Phase" that generates the initial conditions for a tsunami by simulating ocean floor changes due to a forcing event;

Stage 2: A "Propagation Phase" that propagates the generated tsunami across the deep ocean using Nonlinear Shallow Water (NSW) wave equations; and

Stage 3: An "Inundation Phase" that simulates the shallow ocean behavior of a tsunami by extending the NSW calculations using a multi-grid "run-up" algorithm to predict coastal flooding and inundation.

MOST uses the NSW equations, which can be derived as a reduced form of the Navier-Stokes equations. The 2+1 NSW equations, which refer to a model with two horizontal dimensions and one vertical dimension, can be written as follows (Reference 8):

$$h_t + \frac{(uh)_\lambda + (vh\cos\phi)_\phi}{R\cos\phi} = 0$$

$$u_t + \frac{uu_\lambda}{R\cos\phi} + \frac{vu_\phi}{R} + \frac{gh_\lambda}{R\cos\phi} = \frac{gd_\lambda}{R\cos\phi} + fv$$

(1)

$$v_t + \frac{uv_\lambda}{R\cos\phi} + \frac{vv_\phi}{R} + \frac{gh_\phi}{R} = \frac{gd_\phi}{R} - fu$$

where λ is longitude, ϕ is latitude, $h = \eta(\lambda,\phi,t) + d(\lambda(\phi,t)$; $\eta(\lambda,\phi,t)$ is wave amplitude; $d(\lambda,\phi,t)$ is undisturbed water depth, $u(\lambda,\phi,t)$ and $v(\lambda,\phi,t)$ are depth-averaged velocities in longitude and latitude directions, respectively; g is gravitational acceleration; R is the radius of the earth; and f is the Coriolis parameter. Equation (1) is solved

numerically using a finite difference algorithm that splits the NSW equations into a pair of systems (Reference 11).

With respect to wave generation, initial wave dimensions were estimated using the slump center of mass motion model, which is based on curve fits from sliding block experiments (Reference 12 and Reference 13). Source parameters for the East Breaks slump were discussed in the response to Item (6) of RAI 02.04.06-1 (Reference 1) (proposed SSAR Figure 2.4.6-7, attached) and are provided in the proposed text markup for SSAR Subsection 2.4.6.3.4.2. The specific gravity of the slump mass was assumed to be equal to 2 (Reference 12). The 100 m thickness (T) of the East Breaks slump with respect to the 600 m initial depth (d) (T/d=0.17) and the slump thickness relative to the 42 km length (b) of the erosional chute (T/b=0.002) suggests the initial wave height from the East Breaks slump would be relatively small. Using the NGDC bathymetry data (proposed SSAR Figure 2.4.6-7, attached) and the slump center of mass motion model from References 12 and 13, initial wave height for the East Breaks slump was estimated to be 7.9 m. Considering differences between investigators in interpreting landslide dimensions, the estimate of 7.9 m is similar to the "tsunami wave on the order of 7.6 meters" predicted by Trabant et al. (2001) [Reference 2.4.6-3].

Many previous SMF tsunami studies have assumed simplified wave shapes for the initial tsunami wave (Reference 17). For the MOST simulations, specification of an initial deformation condition was based on scaling a dipole wave. A dipole wave is similar to the structure of an N-wave, which is a wave with a leading negative or depression wave followed by a positive elevation wave. Scaling of the wave dimensions into a dipole condition is based on information from other SMF events (Reference 14, Reference 15, and Reference 16) and on estimated source parameters for the East Breaks slump.

SMF events used for initial wave dimensions include the Palos Verdes (PV) landslide in Southern California (Reference 15) and the 1998 Papua New Guinea (PNG) slump in the Sandaun Province (Reference 16). Initial conditions from other events were used as relatively little data exists for SMF tsunamis, and the PV and PNG events have been analyzed extensively by the tsunami community (Reference 17). The PV case was used as a "lower bound" or base case condition. An upper bound condition was developed by assuming an almost instantaneous characteristic time for the SMF. The "upper bound" case was based on the PV case and scaled up by twenty times (PV20). This condition was used to set a reasonable upper limit of wave height for the East Breaks slump. A hypothetical "Monster" condition (hereinafter referred to as "Monster") was also developed as a complementary case for the East Breaks slump to test a very wide initial wave, as opposed to only a tall and steep initial wave. The "Monster" condition has not been simulated or described previously in the tsunami literature.

Initial deformation areas for each simulation (PV, PV20, PNG, and "Monster") are provided in Table 1. Initial deformation areas range from about 387 km^2 to about 9,932 km^2 (149 mi^2 to 3835 mi^2, respectively).

With respect to the propagation phase, a series of nested grids are required for the MOST simulations to maintain resolution of the wave with decreasing water depth since tsunami wavelength becomes shorter during shoaling. Therefore, three grids (A, B and C) were used for the MOST simulations (proposed SSAR Figure 2.4.6-9, attached). The grids were derived from the NGDC topography and bathymetry data (Reference 18). Grid spacing between cell nodes for the A, B, and C grids was 12 arc-seconds (about 360 m), 6 arc-seconds, (about 180 m) and 6 arc-seconds (about 180 m), respectively.

With respect to the inundation phase, MOST uses a moving boundary calculation for estimating tsunami run-up onto dry land. Details of the moving boundary are discussed in Reference 7, Reference 8, and Reference 11. While friction factors are not used in

the propagation phase of MOST, a friction factor must be specified for the inundation phase. Reference 9 states that "several studies show that an unsteady flow during runup is not very sensitive to changes in the roughness coefficient", and that "any moving boundary computation induces numerical friction near the tip of the climbing wave (except in a Lagrangian formulation)."

Sensitivity tests for the MOST inundation friction factor were performed with the PNG simulation case. The inundation friction factor (n^2) was set equal to 0.01, which corresponds to Manning's n=0.1. In addition to Manning's n=0.1 (n^2=0.01) that was used in the MOST simulations, values of Manning's n=0.03 (n^2=0.0009), Manning's n=0.035 (n^2= 0.001225) and Manning's n=0.05 (n^2=0.0025) were also tested for impacts to the results. Lower values of the Manning's coefficient have a negligible impact on flooding near VCS since simulated tsunami inundation is limited primarily to the barrier islands to the east of the Matagorda Island barrier island. The crest elevation of the Matagorda Island barrier island at the coastline near VCS is about 6.6-9.8 ft (2-3 m, respectively) (NAVD 88).

Initial wave dimensions for the PV, PV20, PNG, and "Monster" simulation cases are shown in the attached proposed SSAR Figures 2.4.6-10, 2.4.6-11, 2.4.6-12, and 2.4.6-13, respectively. Initial wave elevations are relative to 0 m (0 ft) MSL. Initial wave trough elevations varied from -7 m to -140 m (-23 ft to -459 ft, respectively) (MSL) and initial wave crest elevations varied from 3 m to 60 m (9.8 ft to 197 ft, respectively) (MSL) (Table 1). Initial wave widths varied from 14 km (8.7 mi) to 136 km (85 mi). The range of initial wave heights and initial wave widths were intended to simulate reasonably probable bounding cases for SMFs that may occur offshore of the South Texas coast.

For all MOST simulations, maximum estimated tsunami runup was 2 m (6.6 ft) (MSL) (Table 1). Plots of maximum wave amplitude for each simulation case (PV, PV20, PNG, and "Monster") are shown in the attached proposed SSAR Figures 2.4.6-10, 2.4.6-11, 2.4.6-12, and 2.4.6-13, respectively. All simulation cases showed significant diffusion of the initial tsunami wave during propagation on the continental shelf (Reference 8). Time series of water surface elevations for a hypothetical buoy location near the coastline of VCS for the PV, PV20, PNG, and "Monster" simulation cases are shown in the attached proposed SSAR Figures 2.4.6-14, 2.4.6-15, 2.4.6-16, and 2.4.6-17, respectively. For wave energy that did reach the South Texas coast, relatively little inundation occurred, with most of the wave energy being reflected by the barrier islands back into the Gulf of Mexico.

The PMT estimate for SSAR Subsection 2.4.6 includes estimates of the 10% exceedance of the astronomical high tide and an estimate of century (one hundred year) sea level rise. As stated in Subsection 2.4.6.5, the 10% exceedance of the astronomical high tide was estimated to be 1.08 m (3.5 ft) MSL based on tide gauge data for NOS Station #8772440 ("Freeport, Texas") and NOS Station #8775870 ("Corpus Christi, Texas"). Long-term sea level rise was estimated to be 0.55 m (1.8 ft) per century. Therefore, the potential maximum water level based on the MOST simulations was estimated to be 2 m (maximum tsunami runup) + 1.08 m (10% exceedance high tide) + 0.55 m (century sea level rise) = 3.59 m (11.8 ft) (MSL) or 3.47 m (11.4 ft) (NAVD 88).

Part (b)

COULWAVE Simulations for Potential Sources at the East Breaks slump and Campeche Escarpment

As stated in the response to Item (1), a recent assessment of tsunami potential in the Gulf of Mexico is provided in Reference 3. Of the four credible SMF sources in the Gulf of Mexico (Northwest Gulf of Mexico, Mississippi Canyon, Florida Margin, and

Campeche Margin), Reference 3 states that the propagation paths that result in the least attenuation of potential tsunamis for the South Texas coast are for the East Breaks and Campeche provinces. Therefore, hydrodynamic simulations were performed in support of Reference 3 for a potential source near the East Breaks slump and for two potential sources at the Campeche Escarpment (i.e., for a 20-km slide width and for a 60-km slide width).

Numerical simulations were performed using the numerical model COULWAVE (Reference 19). As stated in Reference 3 and Reference 19, the numerical model COULWAVE solves the fully nonlinear extended Boussinesq equations on a Cartesian grid. The numerical scheme is based on a fourth order Adams-Bashforth-Moulton predictor-corrector time integration scheme, with spatial derivatives approximated with fourth order, centered finite differences.

With respect to the physical assumptions for the simulations, Reference 3 states that "the purpose of these initial simulations is to provide an absolute upper limit of the tsunami wave height that could be generated" and that "these limiting simulations use physical assumptions that are arguably unreasonable but provide maximum amplitude estimates."

With respect to initial deformation, the time scale of the seafloor motion was assumed to be very small compared to the period of the generated water wave. With this assumption, the free water surface response matches the change in the seafloor profile exactly. Therefore, for estimating the initial free surface condition, Reference 3 states that "the initial pre-landslide bathymetry profile, as estimated by examination of neighboring depth contours, is subtracted by the post (existing) landslide bathymetry profile. This difference surface is smoothed and then used directly as a "hot-start" initial free surface condition in the hydrodynamic model." As with the MOST simulations, the COULWAVE simulations assume initial wave elevations are relative to a still water level of 0 m (0 ft) MSL.

With respect to tsunami propagation, the two horizontal dimension (2HD) COULWAVE simulations were based on a constant spatial grid size of 200 m. Also, bottom roughness was assumed to be negligible in areas that were initially wet (i.e., elevations below 0 ft MSL).

The COULWAVE simulations did not include an inundation phase, stating that "it is most reasonable to analyze the [COULWAVE] 2HD results only to the initial shoreline. The relatively coarse grid size used in the [COULWAVE] 2HD results might cause accuracy degradation during the inundation phase due to poor resolution of shallow bathymetric and on land features."

With respect to the initial wave characteristics for the East Breaks slump tsunami in Reference 3, the initial trough elevation was assumed to be -160 m (-525 ft) (MSL) and the initial crest elevation was assumed to be 100 m (328 ft) (MSL) (Reference 3). The maximum initial wave width was estimated to be about 40 km from Figure 4-2 of Reference 3. The initial deformation area, which was estimated to be about 2,200 km^2 from Figure 4-2 of Reference 3, is significantly larger than the PV, PV20, and PNG initial deformation areas of 411 km^2, 387 km^2, and 879 km^2, respectively, which were used in the MOST simulations (Table 1). However, the initial deformation area of the East Breaks tsunami in COULWAVE is smaller than the initial deformation area of 9,932 km^2 that was used for the "Monster" simulation case in the MOST simulations (Table 1).

With respect to the initial wave characteristics for the Campeche Escarpment tsunami in Reference 3 based on a 20-km slide width (hereinafter referred to as the Campeche Escarpment tsunami), Reference 3 used initial conditions based on the maximum

observed landslide for the Florida Escarpment due to the lack of bathymetry data. Reference 3 states that "as a provisional source for the Campeche Margin, we used initial conditions applicable to the maximum observed landslide along the slope above the Florida Margin, a similar geologic environment. This includes an initial drawdown of 150 m, with a horizontal length scale of 20 km." The initial trough elevation for the Campeche Escarpment tsunami was assumed to be -150 m (-492 ft) (MSL) and the initial crest elevation was assumed to be 150 m (492 ft) (MSL) (Reference 3). The maximum initial wave width is estimated to be about 60 km from Figure 4-4 of Reference 3. The initial deformation area of the Campeche Escarpment, which is estimated to be about 2,000 km^2 from Figure 4-4 of Reference 3, is similar in size to the initial deformation area of the East Breaks slump tsunami of 2,200 km^2. Therefore, the initial deformation area of the Campeche Escarpment tsunami in the COULWAVE simulations is significantly larger than the PV, PV20, and PNG initial deformation areas that were used in the MOST simulations (Table 1). The initial deformation area of the Campeche Escarpment tsunami is smaller than the initial deformation area of 9,932 km^2 that was used for the "Monster" simulation case in the MOST simulations.

Based on the results of synthetic tsunami time series (marigrams) for sources at the East Breaks slump and Campeche Escarpments at an ocean water depth of 50 m (MSL) near Matagorda Bay, Texas (see attached proposed SSAR Figure 2.4.6-18), Reference 2.4.6-18 identifies equal tsunami runup potential from the East Breaks slump and the Campeche Escarpment, stating the following:

> "It was expected that because the propagation distance for Campeche is so much larger than East Breaks (about 700 km longer), the 2D spreading effect is significant, and results in greater attenuation than for the East Breaks scenario. Figure 4-11 [which is reproduced as the attached proposed SSAR Figure 2.4.6-18] compares the ocean surface elevation time series for the offshore Campeche 20-m wide slide and the East Breaks (2HD simulations) at the same 50-m depth offshore location. The general conclusion made from this comparison is that the approaching wave heights for the hypothetical Campeche scenario are comparable to that of the East Breaks scenario, unless it is found that the maximum slide width in the Campeche province is much less than 20 km. Because the properties of the incoming waves are different (leading elevation vs. leading depression), and the uncertainty in the slide parameters, this analysis indicates that East Breaks and Campeche (20 km width) should have equal tsunami potential on the Texas coast."

Reference 3 cited "realistic wave propagation in two horizontal dimensions yielded potential maximum tsunami runup [along the Gulf Coast] of approximately 4 m mean sea level (MSL)." Therefore, as a result of independent hydrodynamic modeling using COULWAVE for the VCS site, Reference 3 states that "the potential maximum water level for the conservative 2HD tsunami over the next century is 4 m (maximum tsunami runup) + 0.45 m (10% exceedance high tide) + 0.59 m (century sea level rise) or approximately 5.0 m (16.5 ft) (MSL)."

Part (c)

PMT estimate from MOST relative to the Minimum Finished Grade of the Power Block

SMF sources located in Mississippi Canyon and Florida Margin are not expected to represent the limiting source mechanism for the PMT for the VCS site due to the orientation and proximity of these sources relative to VCS. As stated in the response to Item (2), Part (a), the potential maximum water level based on the MOST simulations was estimated to be 3.47 m (11.4 ft) (NAVD 88). Therefore, potential maximum water

levels based on MOST simulations, which include inundation modeling, are about 25 m (82 ft) below the minimum finished grade for the power block of 95 ft (NAVD 88).

Based on the above discussion, it is concluded that the flood elevation at VCS due to the postulated PMT will have no flooding impacts on safety-related facilities of VCS. Also, because the VCS site is 36 mi from the coastline, and the minimum finish grade elevation for the plant (95 ft [29.0 meters] NAVD 88) is much higher than the PMT estimate of 11.4 ft (3.47 m) (NAVD 88) obtained with MOST, coincident wind waves are not considered in the analysis since the PMT event will have no flooding impacts on safety-related facilities of VCS.

A conservative estimate of the PMT still water level near the VCS site is about 11.4 ft (3.47 m) (NAVD 88). The minimum finished site grade would be much higher than the PMT water level plus the increase in water level due to coincident wind setup and wave runup as presented in Subsection 2.4.5. Because the flood level due to the postulated PMT event would be much lower than the minimum finished site grade at the power block, debris, waterborne projectiles, sediment erosion and deposition would not have adverse impacts to the safety functions of the station.

RAI References:

1. Exelon Nuclear Texas Holdings, LLC, *Victoria County Station Early Site Permit Application*, Response to Request for Additional Information Letter No. 07, NRC Docket No. 52-042, NP-11-0016, Date: May 5, 2011.

2. Atlantic and Gulf of Mexico Tsunami Hazard Assessment Group, *Evaluation of tsunami sources with the potential to impact the U.S. Atlantic and Gulf coasts – An updated report to the Nuclear Regulatory Commission*: U.S. Geological Survey Administrative Report, August 2008.

3. ten Brink, U., Twichell, D., Lynett, P., Geist, E., Chaytor, J., Lee, H., Buczkowski, B. and C. Flores, 2009, *Regional Assessment of Tsunami Potential in the Gulf of Mexico: U.S. Geological Survey Administrative Report*, Report to the National Tsunami Hazard Mitigation Program, United States Geological Survey, Date: September 2, 2009.

4. British Geological Survey, HR Wallingford, Met Office, Proudman Oceanographic Laboratory, *The Threat Posed by Tsunami to the UK*, Department for Environment, Food and Rural Affairs (DEFRA), Flood Management Division, Date: June 2005.

5. Chaytor, J.D., Twichell, D.C., Lynett, P. and E.L. Geist, 2010, *Distribution and Tsunamigenic Potential of Submarine Landslides in the Gulf of Mexico*, in D.C. Mosher et al. (eds.), Submarine Mass Movements and Their Consequences, Advances in Natural and Technological Hazards Research, Vol. 28, Springer Science + Business Media B.V.

6. South Texas Project Nuclear Operating Company (STPNOC), Final Safety Analysis Report (FSAR), Subsection 2.4S.6, *Probable Maximum Tsunami Hazards*, South Texas Project Units 3 & 4, Combined License Application (COLA), Revision 5.

7. Titov, V.V. and F.I. González, 1997, *Implementation and Testing of the Method of Splitting Tsunami (MOST) Model*, NOAA Technical Memorandum ERL PMEL 112.

8. Titov, V.V. and C.E. Synolakis, 1998, *Numerical Modeling of Tidal Wave Run-up*, Journal of Waterway, Port, Coastal, and Ocean Engineering 124(4): 157-171.

9. González, F.I., Bernard, E., Dunbar, P., Geist, E., Jaffe, B., Kanoglu, U., Locat, J., Mofjeld, H., Moore, A., Synolakis, C.E., Titov, V. and R. Weiss (Science Review Working Group), 2007, *Scientific and Technical Issues in Tsunami Hazard Assessment of Nuclear Power Plant Sites*, NOAA Technical Memorandum OAR PMEL 136.

10. Synolakis, C.E. and E.N. Bernard, 2006, *Tsunami Science Before and Beyond Boxing Day 2004*, Philosophical Transactions of the Royal Society 64: 2231-2265.

11. Titov, V.V., 1997, Numerical Modeling of Long Wave Run-up, Ph.D. Thesis, University of Southern California, Los Angeles, California.

12. Grilli, S.T. and P. Watts, 2005, Tsunami Generation by Submarine Mass Failure, Part I, Modeling Experimental Validation, and Sensitivity Analyses, Journal of Waterway, Port, Coastal, and Ocean Engineering 131(6): 283-297.

13. Watts, P., Grilli, S.T., Tappin, D.R. and G.J. Fryer, 2005, Tsunami Generation by Submarine Mass Failure, Part II, Predictive Equations and Case Studies, Journal of Waterway, Port, Coastal, and Ocean Engineering 131(6): 298-310.

14. Borrero, J.C., Dolan, J.F. and C.E. Synolakis, 2001, *Tsunamis Within the Eastern Santa Barbara Channel*, Geophysical Research Letters 28(4): 643-646.

15. Borrero, J.C., 2002, *Tsunami Hazards in Southern California*, Ph.D. Thesis, University of Southern California, 306 pp.

16. Synolakis, C.E., Bardet, J.-P., Borrero, J.C., Davies, H.L., Okal, E.A., Silver, E.A., Sweet, S., and D.R. Tappin, 2002, *The Slump Origin of the 1998 Papua New Guinea Tsunami*, Proceedings: Mathematical, Physical and Engineering Sciences 458(2020): 763-789.

17. Synolakis, C. E., 2004, Tsunami and Seiche, in Earthquake Engineering Handbook, Chen, W. F. and C. Scawthorn (eds.), CRC Press, 9-1 to 9-90.

18. National Geophysical Data Center (NGDC), 2008, *GEODAS Grid Translator*, National Oceanic and Atmospheric Administration (NOAA), available at http://www.ngdc.noaa.gov/mgg/gdas/gd_designagrid.html, accessed July 26, 2008.

19. Lynett, P. and P.L.F. Liu, 2002, *A numerical study of submarine-landslide-generated waves and run-up*, Proceedings of the Royal Society of London, A, Volume 458, pp. 2885-2910.

Table 1: Initial wave deformation characteristics and maximum runup for East Breaks slump.

Case	Initial Wave Deformation Area [1]	Trough El. (MSL) [2]	Crest El. (MSL) [2]	Trough to Crest Distance	Maximum Runup Elevation (MSL) [2] [3]	HYDRODYNAMIC MODEL
	(sq. km)	(m)	(m)	(m)	(m)	
PV	411	-7	3	7,800	1	MOST[6]
PV20	387	-140	60	7,800	2	MOST[6]
PNG	879	-20	16	5,200	2	MOST[6]
"Monster"	9,932	-38	27	11,700	2	MOST[6]
USGS (2009)[3]	2,200[4]	-160 [4]	100 [5]	37,500[4]	4 [5]	COULWAVE[7]

Notes: (1) Horizontal area of sea surface deformation due to initial wave (relative to 0 ft MSL).

(2) The difference between MSL and NAVD 88 is about 0.4 feet (Elevation MSL = Elevation NAVD 88 + 0.4).

(3) Runup elevation for the South Texas coast.

(4) Estimated from Figure 4-2 of Reference 3.

(5) See Reference 3.

(6) See Reference 7 and Reference 8.

(7) See Reference 19.

Associated ESPA Revisions:

Proposed revisions for SSAR Subsection 2.4.6.3 as shown below incorporate and supersede proposed revisions for SSAR Subsection 2.4.6.3 that were provided in the response to RAI 02.04.06-1 (Reference 1). Proposed SSAR References 2.4.6-13 to 2.4.6-20, which were cited in the response to RAI 02.04.6-1 (Reference 1), are reproduced and incorporated below into this response.

For all model simulations, initial wave elevations are relative to a still water level of 0 m (0 ft) MSL.

In response to this RAI, the first paragraphs of SSAR Subsection 2.4.6, Revision 0 will be revised as follows:

This subsection examines the tsunamigenic sources and identifies the PMT that could affect the Texas Gulf Coast near VCS in an effort to assess the potential safety hazards to the station. It evaluates potential tsunamigenic source mechanisms, source parameters and tsunami propagation and water levels from published studies, and provides information on expected tsunami water levels from Method of Splitting Tsunami (MOST) simulations ~~expected~~ at the site. Historical tsunami events recorded along the Texas Gulf Coast are also reviewed to support the PMT assessment.

In response to this RAI, the third paragraph of SSAR Subsection 2.4.6.1, Revision 0 will be revised as follows:

The major tsunami sources from near-field landslides reside within the Gulf of Mexico. The Gulf of Mexico is characterized by three geologic provinces: the Carbonate, Salt, and Canyon/Fan as shown in Figure 2.4.6-1. Evidence of submarine landslides is recorded in all three geological provinces (Reference 2.4.6-1). The largest submarine failures, including that in the Bryant Canyon and Mississippi Fan, are found in the Canyon/Fan Province that were probably active 7000 years ago. The largest failure in the Salt Province is identified offshore of the Rio Grande River (Reference 2.4.6-1), as shown in Figure 2.4.6-2, in an area known as the East Breaks slump (Reference 2.4.6-3). Reference 2.4.6-1 concludes that while the evaluation of potential tsunamis from large Canyon/Fan landslides would require additional research, landslides in other areas are mainly due to salt movement and may not pose a tsunami hazard for the Gulf Coast. Quantitative information on tsunami generation from these sources is very limited. An extensive literature search revealed ~~reveals one~~a conference paper that provides an estimate of the initial tsunami amplitude for the East Breaks slump landslide, which is given as 7.6 meters (24.9 feet) (Reference 2.4.6-3). Although details of the estimation method were not documented in this paper ~~or supported by other studies~~, a postulated slide in the East Breaks slump is considered as a probable source candidate for the PMT at the Texas Gulf Coast due to its potential to generate high wave amplitude. Additional assessments of potential tsunami amplitude from the East Breaks slump and other Gulf of Mexico sources are provided in Subsection 2.4.6.4.

In response to this RAI, the first four paragraphs of SSAR Subsection 2.4.6.3, Revision 0 will be revised as follows:

2.4.6.3 Source Generator Characteristics

Tsunami source characteristics with potential to affect the US Atlantic and US Gulf Coasts are summarized in Reference 2.4.6-17, Reference 2.4.6-18, tsunami and earthquake databases, and published literature as discussed in the following subsections.~~From the discussion presented above, it is postulated that the tsunami source that could produce a PMT at the Texas Gulf Coast would be a submarine landslide within the Gulf of Mexico. There is no record of tsunamis from this source. The earthquake tsunami sources in the Caribbean Basin frequently generated tsunamis in that region. However, for the Texas Gulf Coast shoreline, the postulated tsunami event due to the hypothetical landslide within the Gulf Basin would be considerably more severe than the earthquake-generated tsunamis.~~

~~The largest landslide complex that was mapped by the USGS in the Gulf Basin is in the middle and upper Mississippi Canyon/Fan province (Reference 2.4.6-1). The area of the landslide complex is estimated to be approximately 23,000 square kilometers (8880 square miles), with a maximum thickness of about 100 meters (328 feet), and a total volume of approximately 1725 cubic kilometers (414 cubic miles). However, the characteristic dimensions of the slide that may be used to generate a tsunami in the Gulf of Mexico are not available (Reference 2.4.6-1). The landslide complex is indicated to have ceased being active by mid-Holocene time.~~

~~Thirty-seven landslides were identified in the Salt province and along the base of the Sigsbee Escarpment (Figure 2.4.6-1) (Reference 2.4.6-1). The largest of these failures occurred in the northwestern Gulf of Mexico, offshore of the Rio Grande River (Figure 2.4.6-2). It was suggested to be the result of a failure of the shelf edge delta forming the river during the last sea level lowstand (Reference 2.4.6-1). The landslide complex, known as the East Breaks slump, is estimated to be 114 kilometers (71 miles) long, 53 kilometers (33 miles) wide, and covers an area of 2250 square kilometers (869 square miles) (Reference 2.4.6-1). However, no further estimates of the slide parameters were established in Reference 2.4.6-1.~~

~~Reference 2.4.6-3 characterizes the East Breaks slump to have a 20 kilometer (12.5 miles) wide head scarp at about the 180 meters (590 feet) isobath, and a slide complex area of approximately 3200 square kilometers (1236 square miles). The estimated length of the slide (erosional) is about 55 kilometers (34 miles), and the maximum thickness of the slump is about 70 meters (230 feet). The total estimated volume of the slide is about 50 to 60 cubic kilometers (12 to 14 cubic miles).~~

2.4.6.3.1 Seismic Tsunamis

Reference 2.4.6-17 states that "tsunamis generated by earthquakes do not appear to impact the Gulf of Mexico coast." For example, in comparison to tsunami runup events that have been documented in the Caribbean (Reference 2.4.6-21), the Texas coast has had relatively few runup events (Table 2.4.6-1). However, tsunamigenic earthquake sources that may affect the Gulf of Mexico are discussed in Reference 2.4.6-17. As stated in Reference 2.4.6-17:

> "Earthquake-generated tsunamis generally originate by the sudden vertical movement of a large area of the seafloor during an earthquake. Such movement is generated by reverse faulting, most often in subduction zones. The Gulf of Mexico basin is devoid of subduction zones or potential sources of large reverse faults. However, the

> Caribbean basin contains two convergence zones whose rupture may affect the Gulf of Mexico, the North Panama Deformation Belt and the Northern South America Convergent Zone."

As discussed in Subsection 2.4.6.1, source areas with potential for tsunamigenesis affecting the US Gulf Coast include the North Panama Deformation Belt and the Northern South-America Convergent Zone (Figure 2.4.6-3). With respect to the North Panama Deformation Belt, Reference 2.4.6-17 states that:

> "the largest segment of the North Panama Deformation Belt is oriented between 60°-77°. The 1882 Panama earthquake appears to have ruptured at least 3/4 of the available length of the convergence zone, and was estimated to have a magnitude of 8. While there was significant tsunami damage locally, there were no reports from the Gulf of Mexico of a tsunami from this earthquake. The low convergent rate (7-11 mm/yr) across the North Panama Deformation Belt supports long recurrence interval for large earthquakes."

The Harvard Centroid-Moment-Tensor (CMT) catalog was searched for potential seismogenic earthquakes in the two source regions of Table 2.4.6-2 (Reference 2.4.6-47). The following criteria were used for searching the CMT catalog within the North Panama Deformation Belt: a date range of January 1, 1976 (the start of the database) through April 30, 2011; latitude from 9° N to 12° N; longitude from 83° W to 77° W; depth from 0 to 1000 km; and a moment magnitude range from 6.5 to 10. The selection of a lower bound moment magnitude of 6.5 is based on criteria from Reference 2.4.6-22 for a threshold moment magnitude of tsunamigenesis from earthquakes. One record was identified in the CMT catalog with these criteria. On April 22, 1991, a M_w=7.6 earthquake occurred at depth of 15 km and at latitude 10.10° N and longitude 82.77° W, located about 20 mi. (32 km) offshore of the town of Limon in Costa Rica. Source parameters for the earthquake were documented as a strike of 103 degrees, a dip of 25 degrees, and a rake of 58 degrees. Source parameters for earthquakes in the North Panama Deformation Belt with moment magnitudes below 6.5 are discussed in Reference 2.4.6-17. With respect to the far-field tsunami hazard on the South Texas coast, these additional sources are not reasonably expected to exceed the tsunamigenic potential of scenarios simulated and presented in Reference 2.4.6-2 and Reference 2.4.6-17.

The following criteria were used for searching the CMT catalog within the Northern South American Convergent Zone: a date range of January 1, 1976 to April 30, 2011; latitude from 11.5° N to 14° N; longitude from 77° W to 64° W; depth from 0 to 1000 km; and moment magnitude range from 6.5 to 10. No records were identified in the CMT catalog with these criteria. By broadening the criteria to include earthquakes from $0<M_w<10$, two records were returned. The moment magnitude of the two earthquakes was 5.1. Moment magnitudes of 5.1 are below the general threshold that is required for seismic tsunamigenesis.

Therefore, the assessment of far-field tsunami hazards in this region was based on tsunami simulations in References 2.4.6-2 and 2.4.6-17. As discussed in Subsection 2.4.6.1, Reference 2.4.6-2 performed tsunami simulations of seismic-borne tsunamis from postulated "worst-case" events using a two-dimensional depth-integrated hydrodynamic model described in Reference 2.4.6-23. The following cases were used in the assessment (Reference 2.4.6-2):

1. M_w=9.0 at 66° W and 18° N (Puerto Rico trench);
2. M_w=8.2 at 85° W and 21° N (Caribbean Sea);
3. M_w=9.0 at 66° W and 12° N (South Caribbean Deformed Belt); and
4. M_w=8.2 at 95° W and 20° N (near Veracruz, Mexico).

The source location of Case #3 above is cited in Reference 2.4.6-2 as the North Panama Deformation Belt, but 66° W and 12° N is located in the South Caribbean Deformed Belt (Reference 2.4.6-17, p. 110).

Source parameters for the simulations in Reference 2.4.6-2 were based on the formulae of Reference 2.4.6-24. For example, source parameters for the Veracruz scenario in Reference 2.4.6-2 are provided in Table 2.4.6-3. Reference 2.4.6-2 states that the model sources were aligned with local strike.

Tsunami simulations in Reference 2.4.6-17 complement earlier work by Reference 2.4.6-2, with Reference 2.4.6-17 stating that:

> "in general, these results are consistent with the findings of Knight (2006) [Reference 2.4.6-2], where the far-field tsunamis generated from earthquakes located beneath the Caribbean Sea are higher along the Gulf coast than the Atlantic coast because of dissipation through the Greater Antilles islands. Conversely, tsunamis generated from earthquakes north of the Greater Antilles are higher along the Atlantic coast than the Gulf coast."

Reference 2.4.6-2 concludes that "sources outside the Gulf are not expected to create a tsunami threatening to the Gulf coast." Reference 2.4.6-2 states that one reason for this conclusion was that "the Atlantic and Gulf coasts are nearly independent since the hydrodynamic connection between basins is through the narrow Straits of Florida and through the Caribbean, where bottom friction losses appear to be large."

Additionally, the largest deepwater wave from the Reference 2.4.6-17 simulations was produced from the north Venezuela subduction zone. The maximum wave height from the north Venezuela subduction zone from a buoy at a depth of 250 m offshore of New Orleans, Louisiana, was estimated to be 6 cm (Reference 2.4.6-17, p. 130, Figure 7-4e, "Station 1").

While tsunamigenic earthquakes within the Gulf of Mexico have not been recorded, Reference 2.4.6-2 included a tsunami simulation assuming a magnitude M_w=8.2 earthquake offshore of Veracruz, Mexico. The resulting wave amplitude at the South Texas coast was about 0.35 m. Intraplate earthquakes are less common than earthquakes occurring on faults near plate boundaries, but several earthquakes in the past three decades had epicenters within the Mississippi Canyon and Fan province (Reference 2.4.6-17). In recent time, the most severe earthquake in this region occurred on September 10, 2006. The moment magnitude was recorded as 5.8. The second largest earthquake in this region occurred on February 10, 2006 with a moment magnitude of 5.2. With respect to the potential for seismic tsunamigenesis within the Gulf of Mexico, Reference 2.4.6-18 states that "there are no significant earthquake sources within the Gulf of Mexico that are likely to generate tsunamis, despite recent seismic activity in the area."

2.4.6.3.2 Seismic Seiches

As stated in Subsection 2.4.6.2, the only documented seismic seiche event on the South Texas coast resulted from the March 27, 1964, Gulf of Alaska earthquake. The moment magnitude for the March 27, 1964, Gulf of Alaska earthquake was 9.2, which is the second largest earthquake in the historical data record (Reference 2.4.6-39). With respect to the generation of seismic seiche waves, Reference 2.4.6-18 states the following:

> "The primary references of seismic seiche waves originating from the March 27, 1964 Gulf of Alaska earthquake are reports by Donn (1964) [Reference 2.4.6-41] and Berninghausen (1968) [Reference 2.4.6-42] who indicated that the waves reached maximum height (peak-trough) of 0.18 m (7 in.) at the Freeport tide gauge station. These reports also refer to eyewitness observations of wave heights up to 2 m from this event."

At the Freeport tide station, the maximum height of 0.18 m (7 in.) that is documented in Reference 2.4.6-41 is similar to the maximum height of 0.20 m (8 in) that is documented in McGarr and Vorhis (1972) (Reference 2.4.6-6).

With respect to generation of a seismic seiche along the South Texas coast, Reference 2.4.6-6 indicated that the horizontal acceleration associated with the seismic surface waves from the Alaska shock appears to have varied markedly within North America according to data from seiches recorded by surface-water gages at the time of the Alaska shock. The amplitude of horizontal acceleration was especially large along the Gulf coast. Reference 2.4.6-6 further states that "thick deposits of sediments of low rigidity along the Gulf coast, for example, are capable of amplifying the horizontal acceleration of surface waves to a considerable extent; this accounts for the concentration of seiches that occurred along the Gulf coast."

The May 22, 1960, earthquake in Chile (M_w=9.5) has the largest moment magnitude in the historical data record (Reference 2.4.6-39). While this earthquake might also have been expected to have caused seiches along the Texas coast, tide gauges along the Gulf Coast did not record any such event. However, a small seiche was observed in Lake Pontchartrain, Louisiana, following the February 27, 2010, Chile (M_w=8.8) earthquake (Reference 2.4.6-40).

Similarly, the February 7, 1812, New Madrid earthquake (M_w=7.8) (Reference 2.4.6-25), which is the largest earthquake recorded in the contiguous United States, produced significant seiches in the Mississippi River and in waterways along the Texas state boundary (Reference 2.4.6-10). However, no records exist to indicate that the 1812 New Madrid earthquake affected the South Texas coast or the Guadalupe River near VCS.

In summary, Reference 2.4.6-17 states that "it is likely that seismic seiche waves resulting from the 1964 Gulf of Alaska earthquake are nearly the highest that can be generated owing to a predominantly continental ray path for seismic surface waves from Alaska to the Gulf Coast."

2.4.6.3.3 Volcanism-based Tsunamis

Reference 2.4.6-17 states that a tsunami hazard does not exist to the US Gulf Coast from volcanism. Previous studies have conjectured that the eruption and collapse of the

Cumbre Vieja volcano on the island of La Palma in the Canary Islands could potentially affect the coast of Florida, with a 25 m wave (Reference 2.4.6-7). A recent assessment of Reference 2.4.6-7 is provided by Reference 2.4.6-17:

> "as envisioned by Ward and Day (2001) [Reference 2.4.6-7], a flank collapse of the volcano may drop a rock volume of up to 500 km^3 into the surrounding ocean. The ensuing submarine slide, which was assumed to propagate at a speed of 100 m/s, will generate a strong tsunami with amplitudes of 25 m in Florida. In addition, they claimed that the collapse of Cumbre Vieja is imminent. In our opinion, the danger to the U.S. Atlantic coast from the possible collapse of Cumbre Vieja is exaggerated."

Further research on the La Palma event indicated that the distribution of slide blocks on the ocean bottom suggests that the collapse of Cumbre Vieja may not have been the result of a single catastrophic event, but the result of several smaller events. A recent report on potential tsunami threats to the United Kingdom concluded that "studies of the offshore turbidites [i.e., poorly sorted sediment that is deposited from a density flow of mixed water and sediment] created by landslides from the flanks of the Canary Islands suggest that these result from multiple landslides spread over periods of several days" and are therefore "likely to create tsunamis of only local concern" (Reference 2.4.6-26).

The National Geophysical Data Center (NGDC) natural hazard database for volcanoes (Reference 2.4.6-19) lists only two volcanoes (Los Atlixcos and San Martin) within 16 km (10 mi) of the present day Gulf of Mexico shoreline. Both volcanoes are located near Veracruz, Mexico. Los Atlixcos is located about 9 km (5.6 mi) from the shoreline and about 975 km (606 mi) from the VCS site. San Martin is located about 13 km (8.0 mi) from the shoreline and about 1127 km (700 mi) from the VCS site. Based on the distance to the shoreline and proximity to VCS, volcanogenic sources near Veracruz, Mexico are not expected to pose a flooding hazard to safety-related functions of VCS.

As no tsunamis have been documented in the Gulf of Mexico as a result of recent volcanic eruptions or associated mass wasting events (gravity-driven mass movement of soil, regolith, or rock moving downslope), this mechanism is not considered further as a potential source of tsunamis along the South Texas coast.

2.4.6.3.4 Submarine Mass Failure (SMF) Tsunamis

Reference 2.4.6-17 cites four credible submarine mass failure (SMF) source areas in the Gulf of Mexico: the Florida Escarpment, Campeche Escarpment, the Mississippi Canyon, and the Northwest Gulf of Mexico (Figure 2.4.6-1). As stated in Subsection 2.4.6.1, these four SMF source areas are located in three geologic provinces: a carbonate province, a canyon to deep-sea fan province, and a salt province.

2.4.6.3.4.1 Carbonate Province

The postulated SMF sources in the carbonate province are located offshore of West Florida and in the Campeche Escarpments north of the Yucatan Peninsula (Reference 2.4.6-17). With respect to the general setting, Reference 2.4.6-17 states the following:

> "During the Mesozoic, an extensive reef system developed around much of the margin of the Gulf of Mexico Basin by the vertical growth of reefs and carbonate

shelf edge banks. This reef system is exposed along the Florida Escarpment and the Campeche Escarpment that fringe the eastern and southern margins of this basin. These escarpments stand as much as 1,500 m above the abyssal plain floor, and have average gradients that commonly exceed 20° and locally are vertical. Reef growth ended during the Middle Cretaceous, and subsequently the platform edges have been sculpted and steepened by a variety of erosional processes."

The largest scar in this region is located along the central part of the West Florida Slope. With respect to estimating maximum landslide scar dimensions for the West Florida Slope (WFS), Reference 2.4.6-43 states the following:

"Mullins et al. (1986) [Reference 2.4.6-44] mapped large collapse scars along the WFS, one of which is 120 km long and 30 km wide, with 300–350 m relief. While the total volume of material removed from this feature is around 1,000 km^3, there were at least 3 generations of failures, with most of the sediment removal occurring prior to the middle Miocene. Along the southern part of the WFS, Doyle and Holmes (1985) [Reference 2.4.6-45] and Twichell et al. (1993) [Reference 2.4.6-46] mapped another extensive area of the slope that has undergone collapse. Here the scarps are still exposed on the seafloor and have 50–150 m relief and are 10–70 km in length. Some of the mass-movement deposits are on the slope above the Florida Escarpment while the remainder were likely transported farther and deposited at the base of the Florida Escarpment. The cross-cutting of the headwall scarps indicates that these landslides are composed of several smaller failure events (Twichell et al. 1993) [Reference 2.4.6-46]."

For the WFS, Reference 2.4.6-43 cites the maximum single event volume as 16 km^3, with a corresponding area of 648 km^2, and an excavation depth of 150 m. The runout distance for the WFS is unknown since the base of the Florida Escarpment is buried under younger Mississippi Fan deposits (SSAR Figure 2.4.6-1) (Reference 2.4.6-17).

No specific information is available on landslide scar dimensions in the Campeche Escarpment. With respect to the general setting, Reference 2.4.6-17 states the following:

"The carbonate platform edge that is exposed along the southern part of the Florida Escarpment and the Campeche Escarpment has been eroded since its initial formation and lagoonal facies are now exposed on the cliff face. The present morphology of these sections of the escarpments is quite different from the northern part of the Florida Escarpment. Here canyons with steep sides and near-vertical headwalls, called box canyons, incise these parts of the escarpments. These box canyons may be the result of dissolution of the limestone by discharge of acidic groundwater at the base of the escarpment in the canyon heads that resulted in collapse of the steep canyon headwalls. A large talus deposit has been identified in seismic profiles along the base of the Campeche Escarpment that was deposited prior to the mid-Cretaceous. The full extent of this deposit is unknown because of limited seismic coverage. Breccia recovered from a [Deep Sea Drilling Project] hole near the base of the Campeche Escarpment presumably is the result of topples and falls from the escarpment face. The amount of material associated with an individual failure is unknown. Talus blocks up to 5-m across and rubble have been observed on the

seafloor along the base of the southern part of the Florida Escarpment which suggests this cliff has recently undergone erosion. The talus deposits in the heads of some of the box canyons cover areas less than 15 km^2, and their thickness is unknown. Published information suggests that the recent falls and topples were limited to the southern part of the Florida Escarpment and perhaps the Campeche Escarpment, but those that have been mapped are of limited aerial extent and are concentrated in the heads of box canyons."

2.4.6.3.4.2 Salt Province

The salt province is located in the northwestern Gulf of Mexico. Reference 2.4.6-17 states that Geologic Long-Range Inclined Asdic (GLORIA) imagery identified 37 SMFs in the salt province and along the base of the Sigsbee Escarpment. With respect to the morphology of the salt province, Reference 2.4.6-17 states the following:

"Salt deposited in the late Jurassic Gulf of Mexico basin, the Louann salt, originally underlay large parts of Louisiana, southern Texas, and the area offshore of Mexico in the Bay of Campeche. As sediment eroded from the North American continent was deposited on this salt sheet throughout the Mesozoic and Cenozoic, the increased load caused the salt to flow with it migrating southward from the source area into the northern Gulf of Mexico. Presently the Louann salt underlies large parts of the northern Gulf of Mexico continental shelf and continental slope. South of Louisiana and Texas, the Sigsbee Escarpment is a pronounced cliff that marks the seaward limit of the shallowest salt tongue. As the salt is loaded, it flows both seaward and also upward through the overlying sediment column as cylindrical salt domes. The morphology of the salt sheet varies considerably across the margin. Salt domes are most common under the continental shelf, and most of the original salt sheet between individual domes in this region has been removed in response to the sediment loading, and migrated farther seaward."

The largest SMF in the Salt province is the East Breaks slump. The East Breaks slump is located about 113 km (70 mi) from the South Texas coast and about 171 km (106 mi) from the VCS site (Figure 2.4.6-8). The coordinates of the slump are approximately 27.57° N and 95.64° W. The slump is comprised of an eastern lobe and a western lobe. Reference 2.4.6-30 states that "the western and eastern lobes are thought to have formed by two different processes, and actually at two different, but relatively close, time periods. The western lobe was formed by slump and debris deposits traveling downslope. The eastern lobe is more consistent with turbidity flow currents in the upper parts of the slide and leveed channels in the middle and lower portions of the slide." Further, Reference 2.4.6-30 states that "the eastern lobe appears more channelized and consists of density flow-type fill with few large slump and intact blocks. The western lobe, therefore, carried the bulk of the failed material and the energy level of the failure was much greater." As the eastern lobe was unlikely to have influenced tsunamigenesis, only the western lobe was used for the present simulations.

The age of the East Breaks slump is not precisely known. Reference 2.4.6-31 states that the most recent mass wasting event responsible for the formation of the western lobe occurred about 16,000 YBP, and after the formation of the bulk of the eastern lobe. Reference 2.4.6-3 states that "the East Breaks Slide is a site of [sea level] lowstand instability, and seismic [reflection] data shows repeated slope failure in this area. During late Quaternary lowstands of sea level, large deltas built up along the Texas-Louisiana

shelf margin, and the present continental shelf [became] exposed as a subaerial coastal plain." Reference 2.4.6-20 also states that "it is clear that most sliding on the Texas-Louisiana slope occurred during the late Pleistocene [c. 10,000 – 29,000 YBP] lowstands of sea level when sedimentation rates on the upper slope were high."

With respect to stability, Reference 2.4.6-17 notes that information on the age of landslides in the salt province is limited. Most landslides appear to have been active during oxygen isotope stages 2, 3, and 4 (18,170-71,000 YBP) when salt movement due to sediment loading was most active. The age of the most recent landslide is less well established. Reference 2.4.6-20 states that that no major SMFs have occurred in the northwestern Gulf of Mexico in the Holocene, with the following:

> "Studies of submarine slides invariably prompt the question: Is the slope now completely stabilized? It is clear that most sliding on the Texas-Louisiana slope occurred during the late Pleistocene lowstands of sea level when sedimentation rates on the upper slope were high. No major Holocene slides have been documented. Low rates of deposition may be a primary reason for the present stability over much of the upper slope, and a further indication that sediments are relatively stable."

However, Reference 2.4.6-17 suggests the occurrence of at least one landslide during the Holocene, with "one unpublished age date of a sample below a thin landslide deposit (<3 m thick) indicates that it is younger than 6,360 YBP." Therefore, no major SMFs have been documented for the salt province in over 6,300 years.

Estimates of dimensions of the East Breaks slump scar dimensions have varied with different investigations. For example, Reference 2.4.6-17 states that the slump "consists of a 20-km wide head scarp initiated along the 150-meter isobath, a 55 km long erosional chute, ending in a 95x30 km accretionary lobe. Total extent of the feature is 160 km from the shelf edge to a depth of 1,500 m" and "slumped deposits extend over a 3,200-km^2 area with a volume on the order of 50-60 km^3." Reference 2.4.6-20 states that "the East Breaks Slide is a prominent mass-transport feature. Revised bathymetry shows that the slide originated on the upper slope (200-1000 m), in front of a sandy late Wisconsinan shelf-margin delta, where the gradient is up to 3°. It was deposited in a middle slope position (1000-1500 m) where the gradient is about 0.5°. Side-scan sonar data indicates that the slide is a strongly backscattering feature extending more than 110 km downslope from the shelf edge." Reference 2.4.6-17 states that "the largest of these failures occurs in the northwestern Gulf of Mexico, is 114 km long, 53 km wide, covers about 2,250 km^2, and has been interpreted to consist of at least two debris flows." Reference 2.4.6-43 estimated a distance of 12 km for the slump width, 50 km for the length of the erosional chute, 160 km for the excavation depth (at the slump headwall), and 130 km for the runout distance from the slump headwall.

Source parameters for the East Breaks slump were also estimated independently as part of hydrodynamic simulations performed for Reference 2.4.6-38. Source parameters were estimated from three-arc-second bathymetry data from the National Geophysical Data Center (NGDC) (Reference 2.4.6-16). Slump width was estimated to be approximately 13.4 km (Figure 2.4.6-7). The length of the erosional chute was estimated to be about 42 km. Based on a transect across the erosional chute, slump thickness was estimated to be about 100 m (see cross-section profile A to A' in Figure 2.4.6-7). With respect to slope, Reference 2.4.6-3 states that "initial failure of the slump took place on very low angle slopes of less than two degrees while present slump deposits have an average

seafloor slope of one-degree." While a vertical drop of 850 m over a length of 42 km indicates a bed slope of approximately 1.1 degrees, a maximum local slope of 2 degrees was used as a conservative estimate. Similarly, initial depth of the slide was estimated conservatively at the depth of the midpoint between the 200 m and 1000 m bathymetry contour elevations. Therefore, initial depth was estimated to be 600 m (i.e., (200 m + 1000 m)/2). Reference 2.4.6-17, citing interpretation of side-scan sonar data by Reference 2.4.6-20, estimated the length of the East Breaks slump as 114 km. Therefore, the total slide length was assumed to be 114 km.

Other SMFs identified in the salt province have areas that are an order of magnitude lower than the East Breaks slump (Reference 2.4.6-17), and are not further considered.

2.4.6.3.4.3 Canyon-To-Fan Province

Three canyon to deep-sea fan systems were formed during the Pliocene and Pleistocene: the Mississippi, Eastern Mississippi, and Bryant systems (SSAR Figure 2.4.6-1). The Mississippi system is the largest of the three systems. Borings and seismic data from the head of Mississippi Canyon indicate that there were alternating episodes of canyon filling and excavation between 19,000 and 7,500 years before the present (YBP). Also, Geologic Long-Range Inclined Asdic (GLORIA) imagery of the Mississippi Fan suggests that this feature consists of at least two separate events (Reference 2.4.6-17). Reference 2.4.6-17 states that the resumption of hemipelagic sedimentation at the head of the Mississippi Canyon by 7500 YBP indicates that the largest of the landslide complexes ceased being active by the middle of the Holocene, i.e., about 5000-7000 years ago. The largest SMF in the complex covers approximately 23,000 km^2 and reaches 100 m in thickness, with a volume estimated to be about 1,750 km^3. GLORIA sidescan sonar data suggests that this feature consists of at least two separate events (Reference 2.4.6-17).

As with the East Breaks slump, estimates of the maximum credible landslide scar dimensions for the Mississippi Fan have varied with different investigations. For the maximum credible single event, Reference 2.4.6-43 reported a volume of 426 km^3, with a corresponding area of 3,687 km^2. Reference 2.4.6-17 and Reference 2.4.6-43 cited the excavation depth as 300 m in the upper canyon, with a runout length of 442 km from the headwall scarp.

The Eastern Mississippi and Bryan Canyon systems are smaller than the Mississippi Canyon system. The Eastern Mississippi system has a deposit that is "approximately 154 km long, as much as 22 km wide, and covers an area of 2,410 km^2" (Reference 2.4.6-17). With respect to the Bryant system, Reference 2.4.6-17 states the following:

> "The Bryant Canyon system was immediately downslope of a shelf edge delta system, and failure of this system has been proposed as the explanation for thick chaotic deposits in mini basins along the path of this canyon system Debris from the failure of the shelf edge delta was transported down the Bryant Canyon system, but these landslide deposits predate and are buried by the smaller landslides off the mini-basin walls."

In response to this RAI, the first paragraph of SSAR Subsection 2.4.6.4, Revision 0 will be revised as follows:

2.4.6.4 Tsunami Analysis

~~The maximum tsunami water level at the Texas Gulf Coast is summarized from the results of published tsunami studies. Detailed water level information for tsunamis generated by potential landslides in the Gulf of Mexico is not available. However, an inference is drawn to computer simulations of a similar landslide scenario for the Currituck slide in the U.S. Atlantic margin near Southern Virginia (Reference 2.4.6-1). Thus, detailed modeling analysis of tsunami amplitude and its propagation are not performed. This qualitative approach is considered adequate in assessing tsunami hazards at the VCS site because the site is not expected to be affected by tsunamis due to its physical location.~~The maximum tsunami water level near the South Texas coastline was evaluated using a hydrodynamic simulation based on the Method of Splitting Tsunami (MOST) model codes (Reference 2.4.6-34), which is discussed in Subsection 2.4.6.4.1. In addition, an independent analysis of maximum tsunami water level near the South Texas coastline was evaluated with the COULWAVE hydrodynamic code (Reference 2.4.6-18), which is discussed in Subsection 2.4.6.4.2.

2.4.6.4.1 MOST Simulations for a Potential Source at the East Breaks slump

Tsunami modeling was conducted for a source originating at the location of the East Breaks slump near the South Texas coast. Hydrodynamic simulations were modeled using a series of codes known as the Method of Splitting Tsunami (MOST) (References 2.4.6-34), which has been subject to extensive validation testing (Reference 2.4.6-22 and Reference 2.4.6-32).

MOST is based on three stages of long wave evolution (Reference 2.4.6-29):

Stage 1: A "Deformation Phase" that generates the initial conditions for a tsunami by simulating ocean floor changes due to a forcing event;

Stage 2: A "Propagation Phase" that propagates the generated tsunami across the deep ocean using Nonlinear Shallow Water (NSW) wave equations; and

Stage 3: An "Inundation Phase" that simulates the shallow ocean behavior of a tsunami by extending the NSW calculations using a multi-grid "run-up" algorithm to predict coastal flooding and inundation.

MOST uses the NSW equations, which can be derived as a reduced form of the Navier-Stokes equations. The 2+1 NSW equations, which refer to a model with two horizontal dimensions and one vertical dimension, can be written as follows (Reference 2.4.6-34):

$$h_t + \frac{(uh)_\lambda + (vh\cos\phi)_\phi}{R\cos\phi} = 0$$

$$u_t + \frac{uu_\lambda}{R\cos\phi} + \frac{vu_\phi}{R} + \frac{gh_\lambda}{R\cos\phi} = \frac{gd_\lambda}{R\cos\phi} + fv$$

(1)

$$v_t + \frac{uv_\lambda}{R\cos\phi} + \frac{vv_\phi}{R} + \frac{gh_\phi}{R} = \frac{gd_\phi}{R} - fu$$

where λ is longitude, ϕ is latitude, $h = \eta(\lambda,\phi,t) + d(\lambda(\phi,t)$; $\eta(\lambda,\phi,t)$ is wave amplitude; $d(\lambda,\phi,t)$ is undisturbed water depth, $u(\lambda,\phi,t)$ and $v(\lambda,\phi,t)$ are depth-averaged velocities in longitude and latitude directions, respectively; g is gravitational acceleration; R is the radius of the earth; and f is the Coriolis parameter. Equation (1) is solved numerically using a finite difference algorithm that splits the NSW equations into a pair of systems and a series of nested grids, which are discussed further below (Reference 2.4.6-29 and Reference 2.4.6-34).

With respect to wave generation, initial wave dimensions were estimated using the slump center of mass motion model, which is based on curve fits from sliding block experiments (Reference 2.4.6-35 and Reference 2.4.6-36). Source parameters for the East Breaks slump were discussed in Subsection 2.4.6.3.4.2. The specific gravity of the slump mass was assumed to be equal to 2 (Reference 2.4.6-35). The 100 m thickness (T) of the East Breaks slump with respect to the 600 m initial depth (d) (T/d=0.17) and the slump thickness relative to the 42 km length (b) of the erosional chute (T/b=0.002) suggests the initial wave height from the East Breaks slump would be relatively small. Using the NGDC bathymetry data (Figure 2.4.6-7) and the slump center of mass motion model from References 2.4.6-35 and 2.4.6-36, initial wave height for the East Breaks slump was estimated to be 7.9 m. Considering differences between investigators in interpreting landslide dimensions, the estimate of 7.9 m is similar to the "tsunami wave on the order of 7.6 meters" predicted by Trabant et al. (2001) (Reference 2.4.6-3).

Many previous SMF tsunami studies have assumed simplified wave shapes for the initial tsunami wave (Reference 2.4.6-33). For the MOST simulations, specification of an initial deformation condition (horizontal area of sea surface deformation from 0 ft MSL due to initial wave) was based on scaling a dipole wave. A dipole wave is similar to the structure of an N-wave, which is a wave with a leading negative or depression wave followed by a positive elevation wave. Scaling of the wave dimensions into a dipole condition is based on information from other SMF events (Reference 2.4.6-27 and Reference 2.4.6-28) and estimated source parameters for the East Breaks slump from Subsection 2.4.6.3.4.2.

SMF events used for initial wave dimensions include the Palos Verdes (PV) landslide in Southern California (Reference 2.4.6-27) and the 1998 Papua New Guinea (PNG) slump in the Sandaun Province (Reference 2.4.6-28). Initial conditions from other events were used as relatively little data exists for SMF tsunamis, and the PV and PNG events have been analyzed extensively by the tsunami community (Reference 2.4.6-33). The PV case was used as a "lower bound" or base case condition. An upper bound condition was developed by assuming an almost instantaneous characteristic time for the SMF. The "upper bound" case was based on the PV case and scaled up by twenty times (PV20). This condition was used to set a reasonable upper limit of wave height for the East Breaks slump. A hypothetical "Monster" condition (hereinafter referred to as "Monster") was also developed as a complementary case for the East Breaks slump to test a very wide initial wave, as opposed to only a tall and steep initial wave. The "Monster" condition has not been simulated or described previously in the tsunami literature.

Initial deformation areas for each simulation (PV, PV20, PNG, and "Monster") are provided in Table 2.4.6-4. Initial deformation areas range from about 387 km^2 to about 9,932 km^2 (149 mi^2 to 3835 mi^2, respectively).

With respect to the propagation phase, a series of nested grids are required for the MOST simulations to maintain resolution of the wave with decreasing water depth since tsunami wavelength becomes shorter during shoaling. Therefore, three grids (A, B and C) were used for the MOST simulations (SSAR Figure 2.4.6-9). The grids were derived from the NGDC topography and bathymetry data (Reference 2.4.6-16). Grid spacing between cell nodes for the A, B, and C grids was 12 arc-seconds (about 360 m), 6 arc-seconds, (about 180 m) and 6 arc-seconds (about 180 m), respectively.

With respect to the inundation phase, MOST uses a moving boundary calculation for estimating tsunami run-up onto dry land. Details of the moving boundary are discussed in Reference 2.4.6-29, Reference 2.4.6-33, and Reference 2.4.6-34. While friction factors are not used in the propagation phase of MOST, a friction factor must be specified for the inundation phase. Reference 2.4.6-22 states that "several studies show that an unsteady flow during runup is not very sensitive to changes in the roughness coefficient," and that "any moving boundary computation induces numerical friction near the tip of the climbing wave (except in a Lagrangian formulation)."

Sensitivity tests for the MOST inundation friction factor were performed with the PNG simulation case. The inundation friction factor (n^2) was set equal to 0.01, which corresponds to Manning's n=0.1. In addition to Manning's n=0.1 (n^2=0.01) that was used in the MOST simulations, values of Manning's n=0.03 (n^2=0.0009), Manning's n=0.035 (n^2= 0.001225) and Manning's n=0.05 (n^2=0.0025) were also tested for impacts to the results. Lower values of the Manning's coefficient have a negligible impact on flooding near VCS since simulated tsunami inundation is limited primarily to the barrier islands to the east of the Matagorda Island barrier island. The crest elevation of the Matagorda Island barrier island at the coastline near VCS is about 6.6-9.8 ft (2-3 m, respectively) (NAVD 88).

Initial wave dimensions for the PV, PV20, PNG, and "Monster" simulation cases are shown in Figures 2.4.6-10, 2.4.6-11, 2.4.6-12, and 2.4.6-13, respectively. Initial wave elevations are relative to a still water level of 0 m (0 ft) MSL. Initial wave trough elevations varied from -7 m to -140 m (-23 ft to -459 ft, respectively) (MSL) and initial wave crest elevations varied from 3 m to 60 m (9.8 ft to 197 ft, respectively) (MSL) (Table 2.4.6-4). Initial wave widths varied from 14 km (8.7 mi) to 136 km (85 mi). The range of initial wave heights and initial wave widths were intended to simulate reasonably probable bounding cases for SMFs that may occur offshore of the South Texas coast.

MOST output includes maximum runup estimates (maximum inland elevation inundated by the tsunami above 0 ft MSL). Maximum runup ranges from 1 to 2 m (3.3 to 6.6 ft, respectively) MSL along the South Texas coast (Table 2.4.6-4). The simulations indicate that a landslide tsunami originating from the East Breaks slump location would be unlikely to cross the barrier islands at the coastline near VCS and produce a runup in excess of 2 m (6.6 ft) (MSL) (Figure 2.4.6-10, Figure 2.4.6-11, Figure 2.4.6-12, and Figure 2.4.6-13).

Plan view plots of maximum wave amplitude relative to the East Breaks slump and the South Texas coast for PV, PV20, PNG, and the "Monster" simulation cases are shown in

Figure 2.4.6-10, Figure 2.4.6-11, Figure 2.4.6-12, and Figure 2.4.6-13, respectively. Time series of water surface elevation above MSL for a buoy location at the coastline near VCS for the PV, PV20, PNG, and "Monster" simulation cases are shown in Figure 2.4.6-14, Figure 2.4.6-15, Figure 2.4.6-16, and Figure 2.4.6-17, respectively.

Maximum drawdown was estimated at a buoy located at depth of 7.7 m and approximately 1 mi offshore of the South Texas coast (Figure 2.4.6-8). At this location, significant drawdown of the water surface below 0 ft MSL occurred for initial negative waves for the PV20 and hypothetical "Monster" scenarios. Maximum drawdown for the PV20 simulation case had a duration of approximately 13 minutes, with a peak negative wave elevation of approximately -1.5 m (-4.9 ft) (MSL). Maximum drawdown for the "Monster" simulation case had a duration of about 11 minutes, with a peak negative wave elevation of about -1 m (-3.3 ft) (MSL). Therefore, maximum drawdown levels are not expected to impact any safety-related facilities at VCS.

2.4.6.4.2 COULWAVE Simulations for Potential Sources at the East Breaks slump and Campeche Escarpment

A recent assessment of tsunami potential in the Gulf of Mexico is provided in Reference 2.4.6-18. Of the four credible SMF sources in the Gulf of Mexico (Northwest Gulf of Mexico, Mississippi Canyon, Florida Margin, and Campeche Margin), Reference 2.4.6-18 states that the propagation paths that result in the least attenuation of potential tsunamis for the South Texas coast are for the East Breaks and Campeche provinces. Therefore, hydrodynamic simulations were performed in support of Reference 2.4.6-18 for a potential source near the East Breaks slump and for two potential sources at the Campeche Escarpment (i.e., for a 20-km slide width and for a 60-km slide width).

Numerical simulations were performed using the numerical model COULWAVE (Reference 2.4.6-37). As stated in Reference 2.4.6-18 and Reference 2.4.6-37, the numerical model COULWAVE solves the fully nonlinear extended Boussinesq equations on a Cartesian grid. The numerical scheme is based on a fourth order Adams-Bashforth-Moulton predictor-corrector time integration scheme, with spatial derivatives approximated with fourth order, centered finite differences.

With respect to the physical assumptions for the simulations, Reference 2.4.6-18 states that "the purpose of these initial simulations is to provide an absolute upper limit of the tsunami wave height that could be generated" and that "these limiting simulations use physical assumptions that are arguably unreasonable but provide maximum amplitude estimates."

With respect to initial deformation, the time scale of the seafloor motion was assumed to be very small compared to the period of the generated water wave. With this assumption, the free water surface response matches the change in the seafloor profile exactly. Therefore, for estimating the initial free surface condition, Reference 2.4.6-18 states that "the initial pre-landslide bathymetry profile, as estimated by examination of neighboring depth contours, is subtracted by the post (existing) landslide bathymetry profile. This difference surface is smoothed and then used directly as a "hot-start" initial free surface condition in the hydrodynamic model." As with the MOST simulations, the COULWAVE simulations assume initial wave elevations are relative to a still water level of 0 m (0 ft) MSL.

With respect to tsunami propagation, the two horizontal dimension (2HD) COULWAVE simulations were based on a constant spatial grid size of 200 m. Also, bottom roughness was assumed to be negligible in areas that were initially wet (i.e., locations with negative bottom elevation).

The COULWAVE simulations did not include an inundation phase, stating that "it is most reasonable to analyze the [COULWAVE] 2HD results only to the initial shoreline. The relatively coarse grid size used in the [COULWAVE] 2HD results might cause accuracy degradation during the inundation phase due to poor resolution of shallow bathymetric and on land features." With respect to the initial wave characteristics for the East Breaks slump tsunami in Reference 2.4.6-18, the initial trough elevation was assumed to be -160 m (-525 ft) (MSL) and the initial crest elevation was assumed to be 100 m (328 ft) (MSL) (Reference 2.4.6-18). The maximum is estimated to be about 40 km from Figure 4-2 of Reference 2.4.6-18. The initial deformation area, which is estimated to be about 2,200 km^2 from Figure 4-2 of Reference 2.4.6-18, is significantly larger than the PV, PV20, and PNG initial deformation areas of 411 km^2, 387 km^2, and 879 km^2, respectively, which were used in the MOST simulations (Table 2.4.6-4). However, the initial deformation area of the East Breaks tsunami in COULWAVE is smaller than the initial deformation area of 9,932 km^2 that was used for the "Monster" simulation case in the MOST simulations (Table 2.4.6-18).

With respect to the initial wave characteristics for the Campeche Escarpment tsunami in Reference 2.4.6-18 based on a 20-km slide width (hereinafter referred to as the Campeche Escarpment tsunami), Reference 2.4.6-18 used initial conditions based on the maximum observed landslide for the Florida Escarpment due to the lack of bathymetry data. Reference 2.4.6-18 states that "as a provisional source for the Campeche Margin, we used initial conditions applicable to the maximum observed landslide along the slope above the Florida Margin, a similar geologic environment. This includes an initial drawdown of 150 m, with a horizontal length scale of 20 km." The initial trough elevation for the Campeche Escarpment tsunami was assumed to be -150 m (-492 ft) (MSL) and the initial crest elevation was assumed to be 150 m (492 ft) (MSL) (Reference 2.4.6-18). The maximum initial wave width is estimated to be about 60 km from Figure 4-4 of Reference 2.4.6-18. The initial deformation area of the Campeche Escarpment, which is estimated to be about 2,000 km^2 from Figure 4-4 of Reference 2.4.6-18, is similar in size to the initial deformation area of the East Breaks slump tsunami of 2,200 km^2. Therefore, the initial deformation area of the Campeche Escarpment tsunami in the COULWAVE simulations is significantly larger than the PV, PV20, and PNG initial deformation areas that were used in the MOST simulations (Table 2.4.6-4). The initial deformation area of the Campeche Escarpment tsunami is smaller than the initial deformation area of 9,932 km^2 that was used for the "Monster" simulation case in the MOST simulations.

Based on the results of synthetic tsunami time series (marigrams) for sources at the East Breaks slump and Campeche Escarpments at an ocean water depth of 50 m (MSL) near Matagorda Bay, Texas (SSAR Figure 2.4.6-18), Reference 2.4.6-18 identifies equal tsunami runup potential from the East Breaks slump and the Campeche Escarpment, stating the following:

> "It was expected that because the propagation distance for Campeche is so much larger than East Breaks (about 700 km longer), the 2D spreading effect is significant, and results in greater attenuation than for the East Breaks scenario.

> Figure 4-11 [which is reproduced as SSAR Figure 2.4.6-18] compares the ocean surface elevation time series for the offshore Campeche 20-m wide slide and the East Breaks (2HD simulations) at the same 50-m depth offshore location. The general conclusion made from this comparison is that the approaching wave heights for the hypothetical Campeche scenario are comparable to that of the East Breaks scenario, unless it is found that the maximum slide width in the Campeche province is much less than 20 km. Because the properties of the incoming waves are different (leading elevation vs. leading depression), and the uncertainty in the slide parameters, this analysis indicates that East Breaks and Campeche (20 km width) should have equal tsunami potential on the Texas coast."

Reference 2.4.6-18 cited "realistic wave propagation in two horizontal dimensions yielded potential maximum tsunami runup [along the Gulf Coast] of approximately 4 m mean sea level (MSL)." Therefore, as a result of independent hydrodynamic modeling using COULWAVE for the VCS site, Reference 2.4.6-18 states that "the potential maximum water level for the conservative 2HD tsunami over the next century is 4 m (maximum tsunami runup) + 0.45 m (10% exceedance high tide) + 0.59 m (century sea level rise) or approximately 5.0 m (16.5 ft) (MSL)."

In response to this RAI, the first six paragraphs of SSAR Subsection 2.4.6.5, Revision 0 will be revised as follows:

2.4.6.5 Tsunami Water Levels

~~There has been no published study that estimates tsunami wave amplitude near the Texas Gulf Coast shoreline as a result of submarine landslides within the Gulf of Mexico. Although the extent of landslides within the Gulf Basin had been mapped, there is not enough information available to characterize the landslide source mechanisms that could be used to generate tsunamis (Reference 2.4.6-1). Reference 2.4.6-3 reports initial tsunami amplitude of about 7.6 meters (24.9 feet) considering the landslide parameters summarized in Subsection 2.4.6.3 for the East Breaks slump. However, this is the only information available on tsunami generation due to landslides in the Gulf of Mexico Basin.~~

~~Reference 2.4.6-1 documents a detailed analysis of the failure mechanism of the Currituck slide, located off the southern Virginia Coast. The results indicate a slide volume between 128 and 165 cubic kilometers (31 and 40 cubic miles) with most of the acceleration phase completed within less than 10 minutes. The average water depth at the base of the slide is estimated to be about 1000 meters (3280 feet). Reference 2.4.6-1 also summarizes preliminary hydrodynamic computations used to estimate the distribution of tsunami amplitude along the nearest Virginia shoreline. The computations were performed using the Cornell University Long and Intermediate Wave Modeling Package (COULWAVE). The COULWAVE package models the propagation and runup of long and intermediate length waves, using fully nonlinear and dispersive wave theory (nonlinear Boussinesq equations). Model simulations were performed for three different geometries of the Currituck slide: down slope sub-event, up slope sub-event, and a composite of the two slide events. The initial and nearshore tsunami amplitudes were found to be the maximum for the composite slide event. Model simulation results, using a failure duration of 10 minutes and a bottom friction coefficient of 2.5x10-3, indicate the maximum initial tsunami amplitude to be approximately 25 meters (82.0 feet) and tsunami amplitude of about 5 meters (16.4 feet) at the nearest shoreline, as shown in Figure 2.4.6-4. The X-axis in Figure 2.4.6-4 represents the cross-shore direction and the Y-axis represents the along-shore direction. The shoreline is represented by X = 100 kilometers in the model. The results also show that the maximum tsunami amplitude would be about 7 meters (23.0 feet) at a water depth of 22 meters (72.2 feet) at a location approximately 20 kilometers (12.5 miles) offshore (as shown in Figure 2.4.6-4(c)).~~

~~As shown in Figure 2.4.6-5, the Currituck landslide area is located approximately 100 kilometers (62.5 miles) offshore, at an average water depth of about 1000 meters (3280 feet). These dimensions are similar to the offshore distance of over 100 kilometers (62.5 miles) and average water depth of about 1000 meters (3280 feet) for the East Breaks slump landslide area (off the mouth of the Rio Grande River in the Gulf of Mexico, as indicated in Figure 2.4.6-6). The width of the shallow continental shelf is also comparable between the two locations, as seen in the figures. The similarities in bathymetric characteristics between the two locations are used to draw inferences for tsunami propagation from the East Breaks slump. The estimated slide volume (50-60 cubic kilometers) and initial tsunami amplitude (7.6 meters) of the East Breaks slump landslide are much smaller than the slide volume and initial tsunami amplitude of the Currituck slide (Reference 2.4.6-3). Accordingly, the maximum tsunami amplitude at the Texas Gulf Coast shoreline is hypothesized to be smaller than the amplitude predicted at the Virginia Coast from the Currituck slide. However, the 5 meter (16.4 feet) tsunami~~

~~amplitude estimated at the shore of the Virginia Coast from the Currituck slide, as shown in Figure 2.4.6-4, is conservatively adopted to represent the PMT wave amplitude at the Texas Gulf Coast shoreline in the assessment of tsunami hazards at the VCS site.~~

~~As shown in Figure 2.4.6-5, the Currituck landslide area is located approximately 100 kilometers (62.5 miles) offshore, at an average water depth of about 1000 meters (3280 feet). These dimensions are similar to the offshore distance of over 100 kilometers (62.5 miles) and average water depth of about 1000 meters (3280 feet) for the East Breaks slump landslide area (off the mouth of the Rio Grande River in the Gulf of Mexico, as indicated in Figure 2.4.6-6). The width of the shallow continental shelf is also comparable between the two locations, as seen in the figures. The similarities in bathymetric characteristics between the two locations are used to draw inferences for tsunami propagation from the East Breaks slump. The estimated slide volume (50-60 cubic kilometers) and initial tsunami amplitude (7.6 meters) of the East Breaks slump landslide are much smaller than the slide volume and initial tsunami amplitude of the Currituck slide (Reference 2.4.6-3). Accordingly, the maximum tsunami amplitude at the Texas Gulf Coast shoreline is hypothesized to be smaller than the amplitude predicted at the Virginia Coast from the Currituck slide. However, the 5 meter (16.4 feet) tsunami amplitude estimated at the shore of the Virginia Coast from the Currituck slide, as shown in Figure 2.4.6-4, is conservatively adopted to represent the PMT wave amplitude at the Texas Gulf Coast shoreline in the assessment of tsunami hazards at the VCS site.~~

~~RG 1.59 requires that the 10 percent exceedance astronomical high tide and sea level anomaly be used as the antecedent water level for the storm surge due to a probable maximum hurricane (PMH) event. The same antecedent water level condition is also used to obtain the PMT maximum water level. The 10 percent exceedance high tide at the Texas Gulf Coast shoreline near the site is estimated to be 3.4 feet (1.04 meters) NGVD 29 or about 3.0 feet (0.92 meters) NAVD 88, the average of the 10 percent exceedance high tides calculated at Freeport, Texas and at Corpus Christi, Texas using historical observed tidal records at the two stations. Additionally, the PMH event considers a long-term sea level rise of 1.8 feet (0.55 meters) for the next 100 years as described in Subsection 2.4.5. Combining the 10 percent exceedance high tide (3.0 feet) and the long-term sea level rise (1.8 feet) with the postulated conservative tsunami amplitude at the Texas Gulf Coast near the VCS site (16.4 feet), the PMT maximum water level at the shoreline is 21.2 feet (6.5 meters) NAVD 88.~~

~~The Guadalupe River near the VCS site has natural levees and wide floodplains with a maximum elevation of approximately 20 feet (6.1 meters) NAVD 88. According to the National Weather Services floodmark, a historical high water level of 33.92 feet (10.34 meters) above National Geodetic Vertical Datum of 1929 (NGVD 29) was recorded in Bloomington, Texas during the flood of October 20, 1998 (Reference 2.4.6-11). To estimate the PMT water level at the site, it is conservatively assumed that the antecedent water level in the river would be at its historical flood stage of 33.92 feet (10.34 meters) NGVD 29, which is equivalent to 33.5 feet (10.22 meters) NAVD 88, the PMT wave amplitude at the Gulf Coast shoreline would be 21.2 feet (6.5 meters), and the tsunami wave would propagate inland without any dispersion or dissipation. Thus, the maximum PMT still water level near the site would be about (33.5 + 21.2 ~) 55.0 feet (16.8 meters) NAVD 88. The PMT still water level would be approximately 40.0 feet (12.2 meters) below the minimum finished site grade elevation of the power block of VCS. Coincident wind setup and wave runup, as presented in Subsection 2.4.5, would not affect the power block of the site. Therefore, it is concluded that the PMT event at the Texas Gulf Coast would not cause any flooding of the power block.~~

~~The PMT event could also induce a water surface drawdown at the Texas Gulf Coast shoreline. For the Virginia Coast, a maximum tsunami drawdown (trough) of about 3.5 meters (11.5 feet) at a water depth of 22 meters (72.2 feet) was reported (Reference 2.4.6-1). A similar low water condition may also be considered for the Texas Gulf Coast, similar to the tsunami amplitude estimate. Because of the presence of barrier islands (Matagorda Island) on the shoreline near the site, the drawdown water level at the shoreline would have limited effect on the water level within San Antonio Bay. Low water level in the Guadalupe River near the site is controlled by the river flow and by the regulation of the Lower Guadalupe River Saltwater Barrier and Diversion Dam near Tivoli, Texas. The 50-foot long inflatable dam was designed to prevent salt water intrusion up the river and to maintain the pool level for the diversion of river water to the GBRA canal system (Reference 2.4.6-12). The saltwater barrier is inflated if the water level in the Guadalupe River at Tivoli falls below 4.0 feet (1.2 meters) above mean sea level or NGVD 29, which is equivalent 3.6 feet (1.1 meters) NAVD 88. Consequently, the effect of tsunami drawdown upstream of the saltwater barrier would be prevented by the operation of the barrier dam. Furthermore, because VCS does not rely on the Guadalupe River or its water supply to perform any plant safety-related function, low water.~~ As discussed in Subsection 2.4.6.3, subaerial landslides, volcanogenic sources, and near-field intraplate earthquakes are unlikely to be the causative tsunami generator for damaging tsunamis in the Gulf of Mexico region. Reference 2.4.6-17 states that "tsunamis generated by earthquakes do not appear to impact the Gulf of Mexico coast." Simulations by Reference 2.4.6-2 of postulated "worst-case" seismic events reported a tsunami near VCS with a shoreline amplitude of 0.15 m (MSL).

The East Breaks slump was selected as the PMT source based on its proximity, and dimensions and orientation relative to the VCS site. For initial waves with trough elevations and crest elevations ranging from –140 m (-459 ft) (MSL) to 60 m (197 ft) (MSL), respectively, and initial wave widths ranging from 14 km (8.7 mi) to 136 km (85 mi) (Table 2.4.6-4), respectively, maximum runup elevations from the MOST simulations did not exceed 2 m (MSL) for about 106 mi of the South Texas coastline. All simulated scenarios showed significant diffusion of the initial tsunami wave at the continental shelf. For the wave energy that did reach the South Texas coast, most of the energy was reflected by the barrier islands back into the Gulf of Mexico.

Using the MOST simulation results for maximum tsunami runup and alternative estimates for 10% exceedance of high tide and century sea level rise, the potential maximum water level can also be estimated as 2 m (maximum tsunami runup) + 1.08 m (10% exceedance high tide) + 0.55 m (century sea level rise) = 3.59 m (11.8 ft) (MSL) or 3.47 m (11.4 ft) (NAVD 88). Therefore, potential maximum water levels based on MOST simulations, which include inundation modeling, are about 25 m (82 ft) below the minimum finished grade for the power block of 95 ft (NAVD 88).

Based on the above discussion, it is concluded that the flood elevation at VCS due to the postulated PMT will have no flooding impacts on safety-related facilities of VCS. Also, because the VCS site is 36 mi from the coastline, and the minimum finish grade elevation for the plant (95 ft [29.0 m] NAVD 88) is much higher than the PMT estimate of 11.4 ft (3.47 m) (NAVD 88) obtained with MOST, coincident wind waves are not considered in the analysis since the PMT event will have no flooding impacts on safety-related facilities of VCS.

In response to this RAI, the first paragraph of SSAR Subsection 2.4.6.7, Revision 0 will be revised as follows:

A ~~very~~ conservative estimate of the PMT still water level ~~in the Guadalupe River~~ near the VCS site is about ~~55.0 feet (16.8 meters) NAVD 88~~11.4 ft (3.47 m) (NAVD 88). The minimum finished site grade of 95 feet (29.0 meters) NAVD 88 for the power block of the station would be much higher than this PMT water level plus the increase in water level due to coincident wind setup and wave runup as presented in Subsection 2.4.5. Because the flood level due to the postulated PMT event would be much lower than the minimum finished site grade at the power block, debris, waterborne projectiles, sediment erosion and deposition would not have adverse impacts to the safety functions of the station.

Proposed SSAR References 2.4.6-13 to 2.4.6-20, which were added in response to RAI 02.04.6-1 (Reference 1), are reproduced below for this response. In response to this RAI, SSAR Subsection 2.4.6.8, Revision 0 will be revised by adding the following references after Reference 2.4.6-12:

2.4.6-13 McCann, W., *Estimating the threat of tsunamigenic earthquakes and earthquake induced-landslide tsunami in the Caribbean*, Caribbean Tsunami Hazards, Proceedings of the NSF Caribbean Tsunami Workshop, Mercado-Irizarry, A. and Liu, P. (eds.), 43–65, World Scientific Publishing Co. Pte. Ltd., Singapore, 2006.

2.4.6-14 Kammerer, A., ten Brink, U., and Titov, V., *Overview of the U.S. Nuclear Regulatory Commission collaborative research program to assess tsunami hazard for nuclear power plants on the Atlantic and Gulf coasts*, The 14th World Conference on Earthquake Engineering, October 12–17, 2008, Beijing, China.

2.4.6-15 Pararas-Carayannis, G., *Volcanic tsunami generating source mechanisms in the eastern Caribbean region*, Science of Tsunami Hazards, 22(2): 74–114, 2004.

2.4.6-16 National Geophysical Data Center (NGDC), 2008, GEODAS Grid Translator, National Oceanic and Atmospheric Administration (NOAA), available at http://www.ngdc.noaa.gov/mgg/gdas/gd_designagrid.html, accessed July 26, 2008.

2.4.6-17 Atlantic and Gulf of Mexico Tsunami Hazard Assessment Group, 2008, *Evaluation of Tsunami Sources with the Potential to Impact the U.S. Atlantic and Gulf Coasts - A Report to the Nuclear Regulatory Commission*: U.S. Geological Survey Administrative Report, Revision: August 22, 2008.

2.4.6-18 ten Brink, U., Twichell, D., Lynett, P., Geist, E., Chaytor, J., Lee, H., Buczkowski, B. and C. Flores, 2009, *Regional Assessment of Tsunami Potential in the Gulf of Mexico*, U.S. Geological Survey Administrative Report, Report to the National Tsunami Hazard Mitigation Program, United States Geological Survey, Date: September 2, 2009.

2.4.6-19 National Geophysical Data Center (NGDC), 2010, *Volcano Location Database Search*, National Oceanic and Atmospheric Administration (NOAA), available at http://www.ngdc.noaa.gov/nndc/struts/form?t=102557&s=5&d=5, accessed May 2, 2011.

2.4.6-20 Rothwell, R.G., Kenyon, N.H. and B.A. McGregor, *Sedimentary Features of the South Texas Continental Slope as Revealed by Side-Scan Sonar and High-Resolution Seismic Data*, The American Association of Petroleum Geologists Bulletin 75(2): 298-312, 1991.

2.4.6-21 Parsons, T. and E.L. Geist, 2009, *Assessment of Source Probabilities for Potential Tsunamis Affecting the U.S. Atlantic Coast*, Marine Geology 264(1-2): 98-108.

2.4.6-22 González, F.I., Bernard, E., Dunbar, P., Geist, E., Jaffe, B., Kanoglu, U., Locat, J., Mofjeld, H., Moore, A., Synolakis, C.E., Titov, V. and R. Weiss (Science Review Working Group), 2007, *Scientific and Technical Issues in Tsunami Hazard Assessment of Nuclear Power Plant Sites*, NOAA Technical Memorandum OAR PMEL 136.

2.4.6-23 Kowalik, Z., Knight, W., Logan, T. and P. Whitmore, 2005, *Numerical Modeling of the Global Tsunami: Indonesian Tsunami of 26 December 2004*, Science of Tsunami Hazards 23(1): 40-56.

2.4.6-24 Okada, Y., 1985, *Surface Deformation Due to Shear and Tensile Faults in a Half-Space*, Bulletin of the Seismological Society of America 75(4): 1135-1154.

2.4.6-25 Bakun, W.H. and M.G. Hopper, 2004, *Magnitudes and Locations of the 1811-1812 New Madrid, Missouri, and the 1886 Charleston, South Carolina, Earthquakes*, Bulletin of the Seismological Society of America 94(1): 64-75.

2.4.6-26 British Geological Survey, HR Wallingford, Met Office, Proudman Oceanographic Laboratory, *The Threat Posed by Tsunami to the UK*, Department for Environment, Food and Rural Affairs (DEFRA), Flood Management Division, Date: June 2005.

2.4.6-27 Borrero, J.C., 2002, *Tsunami Hazards in Southern California*, Ph.D. Thesis, University of Southern California.

2.4.6-28 Synolakis, C.E., Bardet, J.-P., Borrero, J.C., Davies, H.L., Okal, E.A., Silver, E.A., Sweet, S., and D.R. Tappin, 2002, *The Slump Origin of the 1998 Papua New Guinea Tsunami*, Proceedings: Mathematical, Physical and Engineering Sciences 458(2020): 763-789.

2.4.6-29 Titov, V.V. and F.I. González, 1997, *Implementation and Testing of the Method of Splitting Tsunami (MOST) Model*, NOAA Technical Memorandum ERL PMEL 112.

2.4.6-30 Hoffman, J.S., Kaluza, M.J., Griffiths, R., Hall, J. and T. Nguyen, 2004, *Addressing the Challenges in the Placement of Seafloor Infrastructure on the East Breaks Slide-A Case Study: The Falcon Field (EB 579/623)*, Northwestern Gulf of Mexico, Offshore Technology Conference 16748.

2.4.6-31 Piper, J.N. and W.E. Behrens, 2003, *Downslope Sediment Transport Processes and Sediment Distributions at the East Breaks, northwest Gulf of Mexico*, in Proceedings of the 23rd Annual Gulf Coast Section SEPM Research Conference, Houston, TX, pp. 359-385.

2.4.6-32 Synolakis, C.E. and E.N. Bernard, 2006, *Tsunami Science Before and Beyond Boxing Day 2004*, Philosophical Transactions of the Royal Society 64: 2231-2265.

2.4.6-33 Synolakis, C. E., 2004, *Tsunami and Seiche*, in Earthquake Engineering Handbook, Chen, W. F. and C. Scawthorn (eds.), CRC Press, 9-1 to 9-90.

2.4.6-34 Titov, V.V. and C.E. Synolakis, 1998, *Numerical Modeling of Tidal Wave Run-up*, Journal of Waterway, Port, Coastal, and Ocean Engineering 124(4): 157-171.

2.4.6-35 Grilli, S.T. and P. Watts, 2005, Tsunami Generation by Submarine Mass Failure, Part I, Modeling Experimental Validation, and Sensitivity Analyses, Journal of Waterway, Port, Coastal, and Ocean Engineering 131(6): 283-297.

2.4.6-36 Watts, P., Grilli, S.T., Tappin, D.R. and G.J. Fryer, 2005, *Tsunami Generation by Submarine Mass Failure, Part II, Predictive Equations and Case Studies*, Journal of Waterway, Port, Coastal, and Ocean Engineering 131(6): 298-310.

2.4.6-37 Lynett, P. and P.L.F. Liu, 2002, *A numerical study of submarine-landslide-generated waves and run-up*, Proceedings of the Royal Society of London, A, Volume 458, pp. 2885-2910.

2.4.6-38 South Texas Project Nuclear Operating Company (STPNOC), Final Safety Analysis Report (FSAR), *Subsection 2.4S.6, Probable Maximum Tsunami Hazards*, South Texas Project Units 3 & 4, Combined License Application (COLA), Revision 5.

2.4.6-39 U.S. Geological Survey, Earthquake Hazards Program, *Historic World Earthquakes, Sorted by Magnitude*, accessed May 26, 2011, available at http://earthquake.usgs.gov/earthquakes/world/historical_mag.php.

2.4.6-40 U.S. Geological Survey, Earthquake Hazards Program, *Magnitude 8.8 - Offshore Bio-Bio, Chile, 2010 February 27 06:34:14 UTC*, accessed May 26, 2011, available at http://earthquake.usgs.gov/earthquakes/eqinthenews/2010/us2010tfan/#summary.

2.4.6-41 Donn, W.L., 1964, *Alaskan earthquake of 27 march 1964: Remote seiche stimulation*: Science 145: 261-262.

2.4.6-42 Berninghausen, W.H., 1968, *Tsunamis and Seismic Seiches Reported from the Western North and South Atlantic and the Coastal Waters of Northwestern Europe*: Naval Oceanographic Office IR No. 68-85 [Informal Report].

2.4.6-43 Chaytor, J.D., Twichell, D.C., Lynett, P. and E.L. Geist, 2010, *Distribution and Tsunamigenic Potential of Submarine Landslides in the Gulf of Mexico*, in D.C. Mosher et al. (eds.), Submarine Mass Movements and Their Consequences, Advances in Natural and Technological Hazards Research, Vol. 28, Springer Science + Business Media B.V.

2.4.6-44 Mullins, H.T., Gardulski, A.F. and A.C. Hine, 1986, *Catastrophic Collapse of the West Florida Carbonate Platform Margin*, Geology 14: 167-170.

2.4.6-45 Doyle L.J. and C.W. Holmes, 1985, *Shallow Structure, Stratigraphy, and Carbonate Sedimentary Processes of West Florida Continental Slope*, American Association of Petroleum Geologists Bulletin 69:1133–1144.

2.4.6-46 Twichell, D.C., Valentine, P.C., and L.M. Parson, 1993, *Slope Failure of Carbonate Sediment on the West Florida Slope*, in Schwab, W.C., Lee, H.J., and Twichell, D.C. (eds.), Submarine Landslides: Selected Studies in the U.S. Exclusive Economic Zone, U.S. Geological Survey Bulletin 2002: 69-78.

2.4.6-47 *Global Centroid Moment Tensor* (CMT) database, Available at http://www.globalcmt.org/, accessed May 13, 2011.

In response to this RAI, Table 2.4.6-2, Table 2.4.6-3, and Table 2.4.6-4 will be added, respectively:

Table 2.4.6-2. Areas of potential seismic tsunamigenesis in the Caribbean (Reference 2.4.6-17).

Caribbean Source	Latitude (° N)	Longitude (° W)
North Panama Deformation Belt	9-12	83-77
Northern South American Convergent Zone	11.5-14	77-64

Table 2.4.6-3. Source parameters for Veracruz scenario.

Epicenter	M_w	Rupture Length (km)	Width (km)	Depth (km)	Strike (deg.)	Dip (deg.)	Rake (deg.)	Max slip (m)
20° N, 265° E	8.2	200	70	5	135	20	90	2

Table 2.4.6-4: Initial wave deformation characteristics and maximum runup elevation based on a tsunamigenic source at the East Breaks slump.

Case	Initial Wave Deformation Area [1]	Trough El. (MSL) [2]	Crest El. (MSL) [2]	Trough to Crest Distance	Maximum Runup Elevation (MSL) [2] [3]	HYDRODYNAMIC MODEL
	(sq. km)	(m)	(m)	(m)	(m)	
PV	411	-7	3	7,800	1	MOST[6]
PV20	387	-140	60	7,800	2	MOST[6]
PNG	879	-20	16	5,200	2	MOST[6]
"Monster"	9,932	-38	27	11,700	2	MOST[6]
USGS (2009)[3]	2,200[4]	-160 [4]	100 [5]	37,500[4]	4 [5]	COULWAVE[7]

Notes: (1) Horizontal area of sea surface deformation due to initial wave (relative to 0 ft MSL).

(2) The difference between MSL and NAVD 88 is about 0.4 feet (Elevation MSL = Elevation NAVD 88 + 0.4).

(3) Runup elevation for the South Texas coast.

(4) Estimated from Figure 4-2 of Reference 2.4.6-18.

(5) See Reference 2.4.6-18.

(6) See Reference 2.4.6-29 and Reference 2.4.6-34.

(7) See Reference 2.4.6-37.

SSAR Figure 2.4.6-7, which was added in response to RAI 02.04.6-1 (Reference 1), is reproduced in this response. In response to this RAI, SSAR Figure 2.4.6-8, SSAR Figure 2.4.6-9, SSAR Figure 2.4.6-10, SSAR Figure 2.4.6-11, SSAR Figure 2.4.6-12, SSAR Figure 2.4.6-13, SSAR Figure 2.4.6-14, SSAR Figure 2.4.6-15, SSAR Figure 2.4.6-16, SSAR Figure 2.4.6-17, and SSAR Figure 2.4.6-18 will be added:

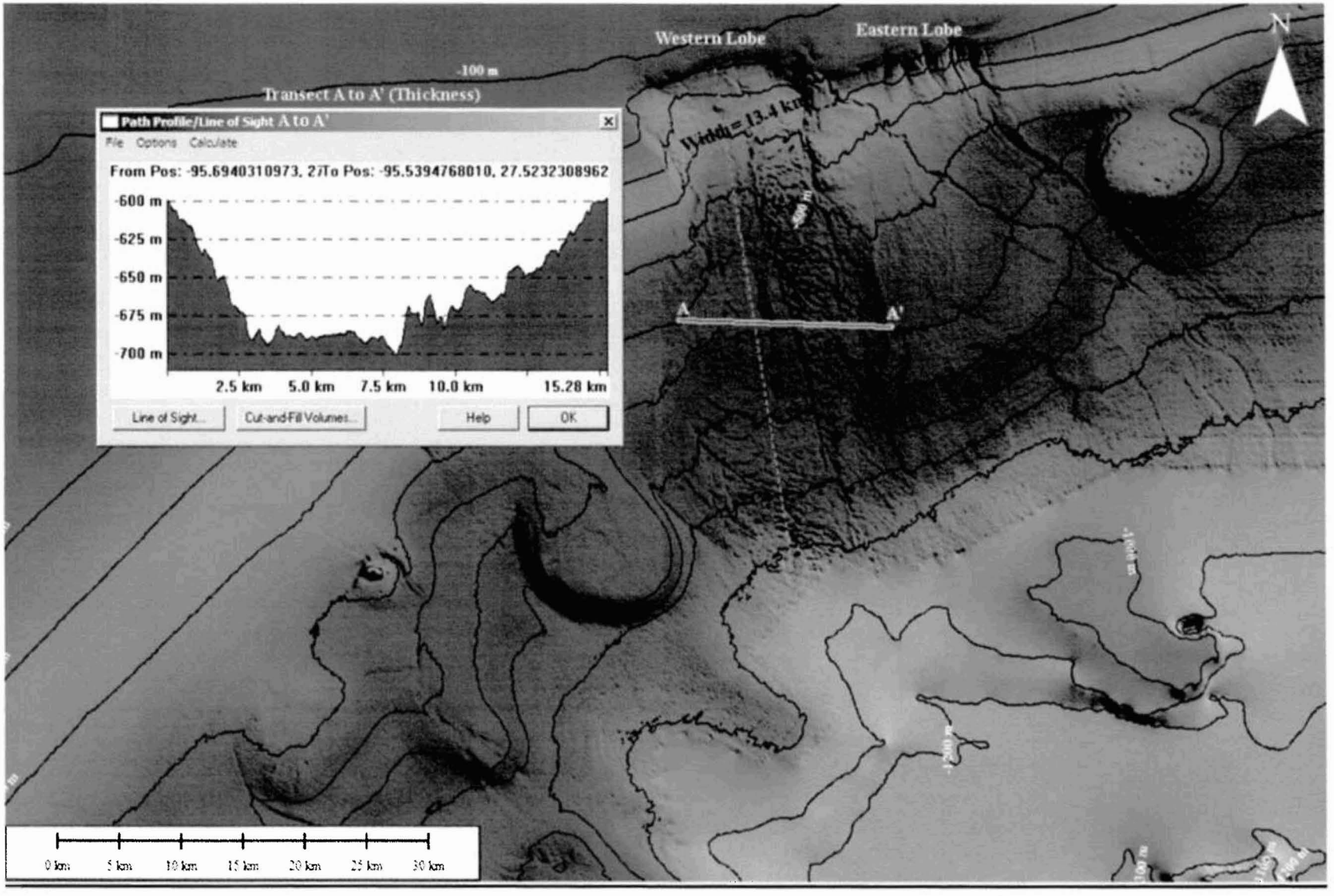

Figure 2.4.6-7 Source parameters for East Breaks slump - Bathymetry elevations are relative to MSL. (Source of bathymetry data: Reference 2.4.6-16)

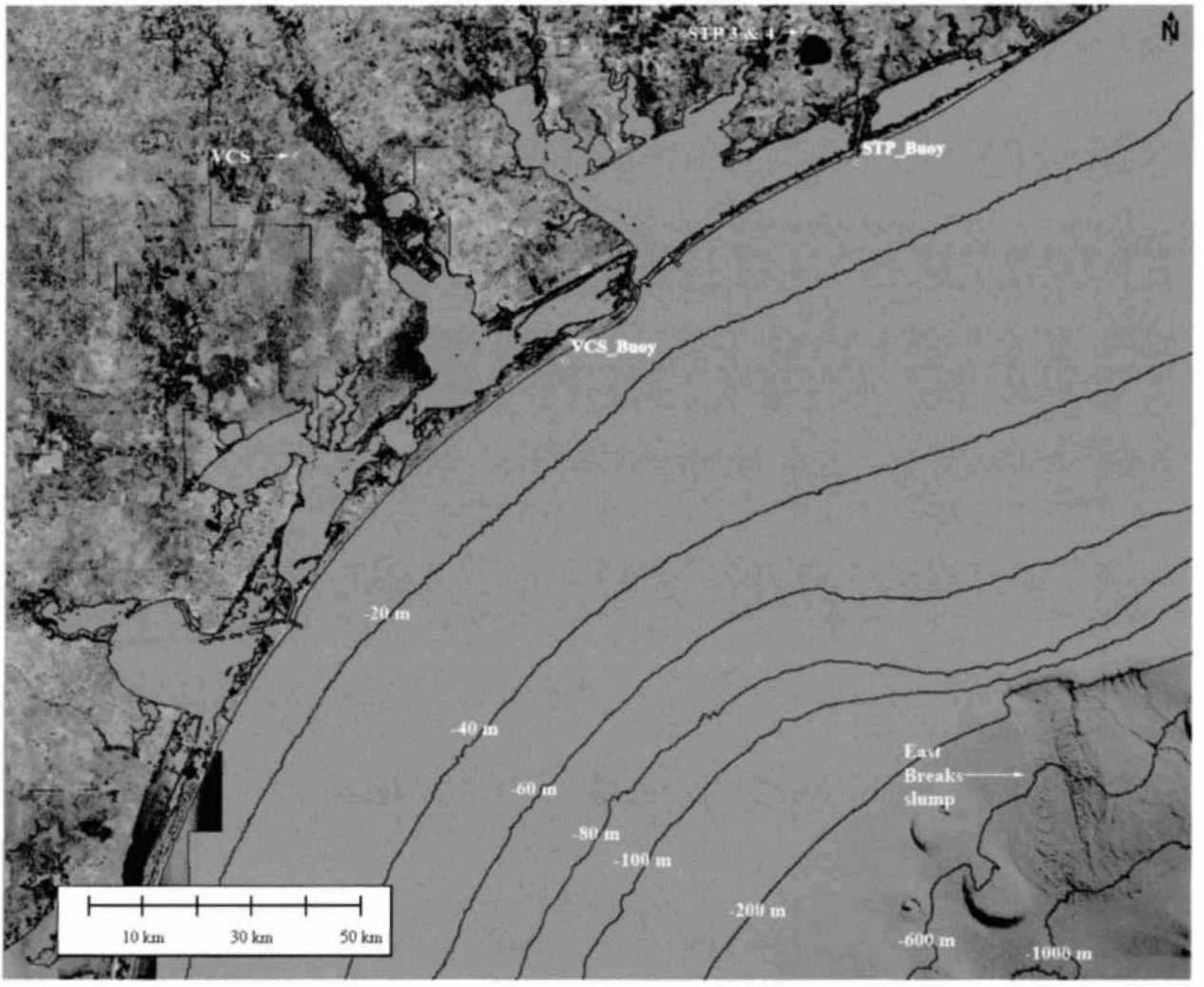

Figure 2.4.6-8 Site location map showing VCS relative to STP 3 & 4, the East Breaks slump, and hypothetical buoy locations (VCS_Buoy and STP_Buoy) that were used for plotting time history for MOST model simulations. Bathymetry elevations are relative to MSL.

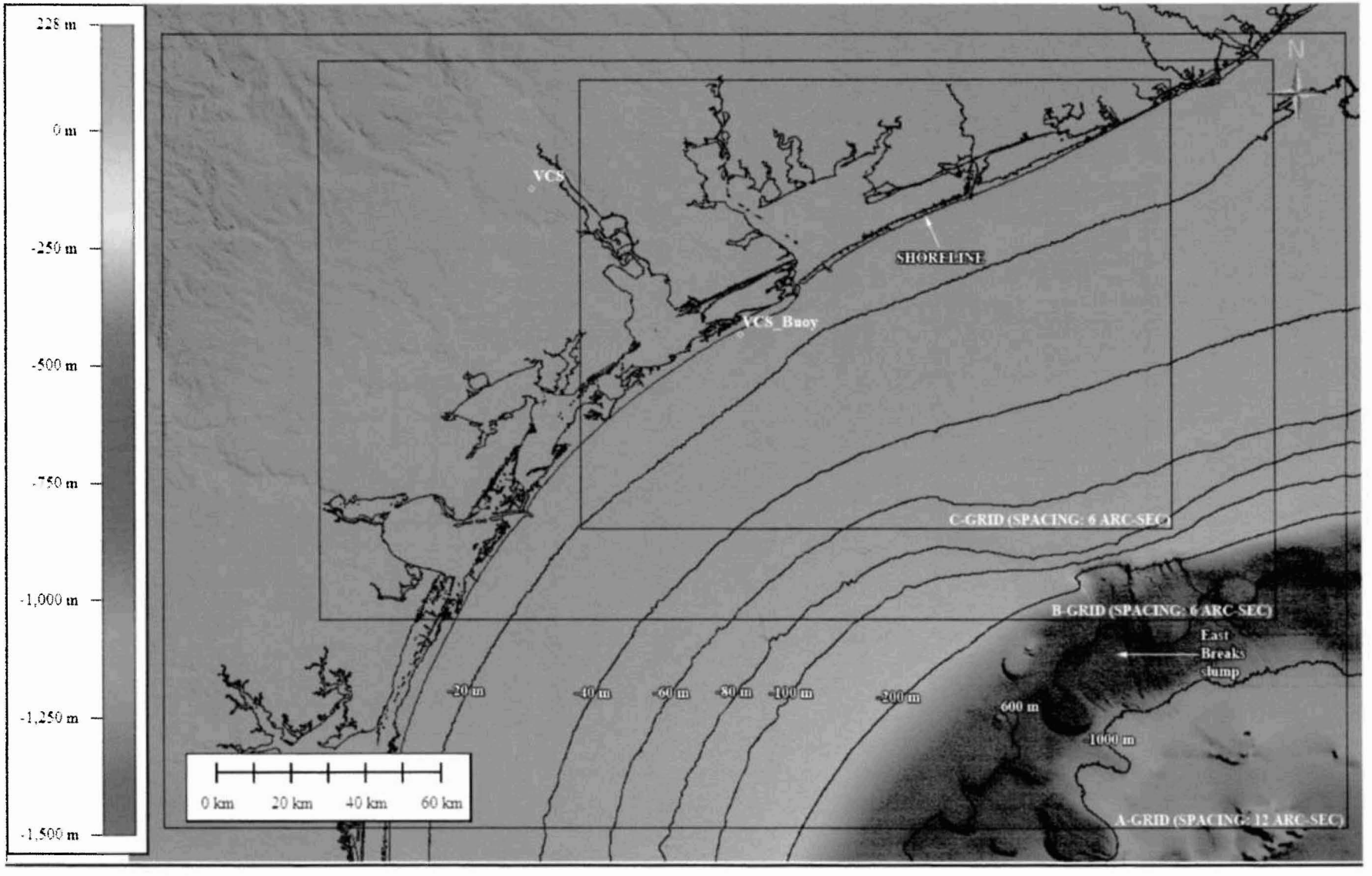

Figure 2.4.6-9 Plan view of nested grids (A, B, and C) used for MOST simulations. Ground elevations and bathymetry elevations are relative to MSL (Source: Reference 2.4.6-16).

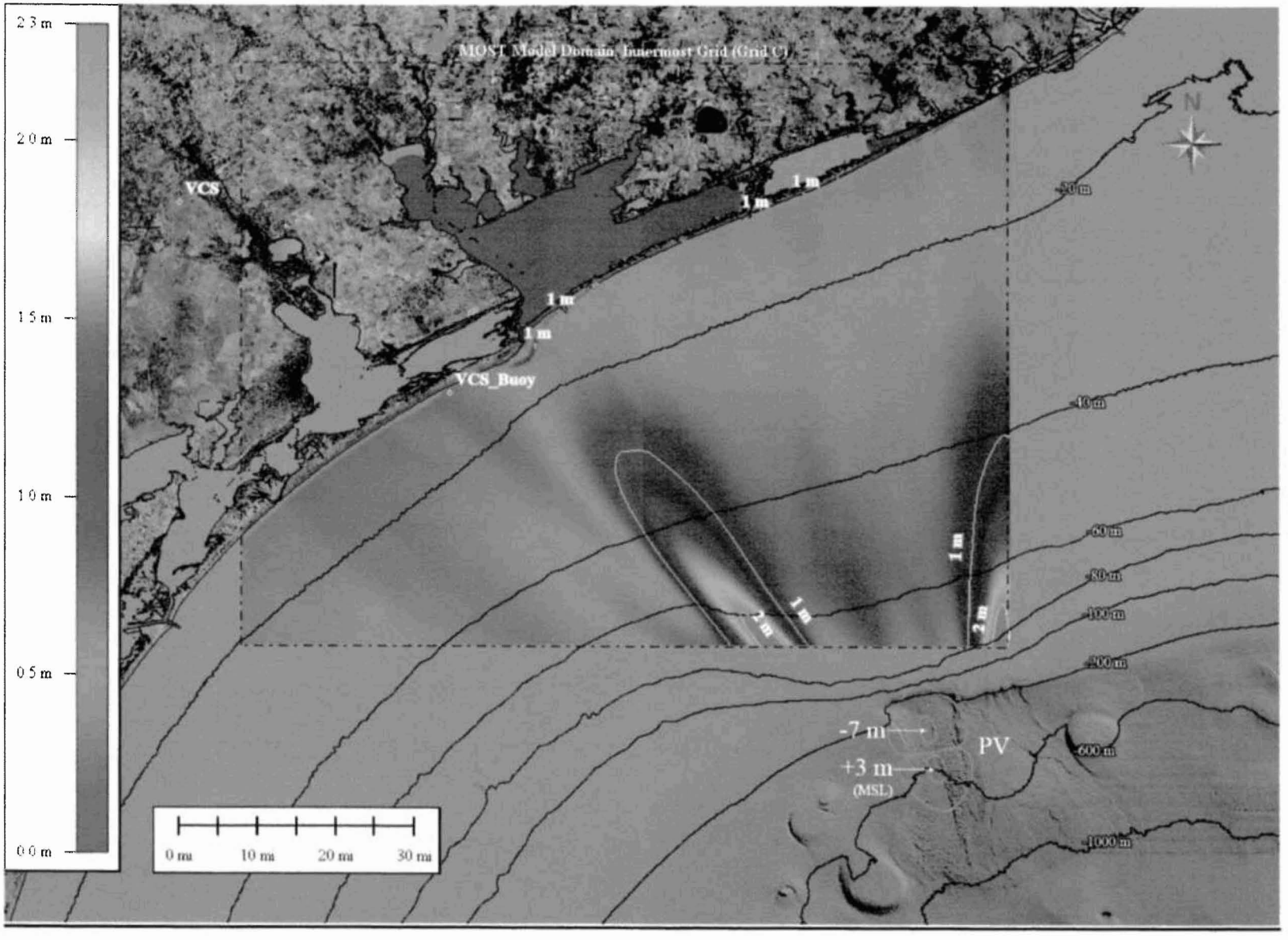

Figure 2.4.6-10 Maximum water surface elevations (MSL) for simulation case PV. Maximum tsunami runup elevation: 1 m (MSL), with negligible inundation past the barrier islands. Bathymetry elevations are relative to MSL.

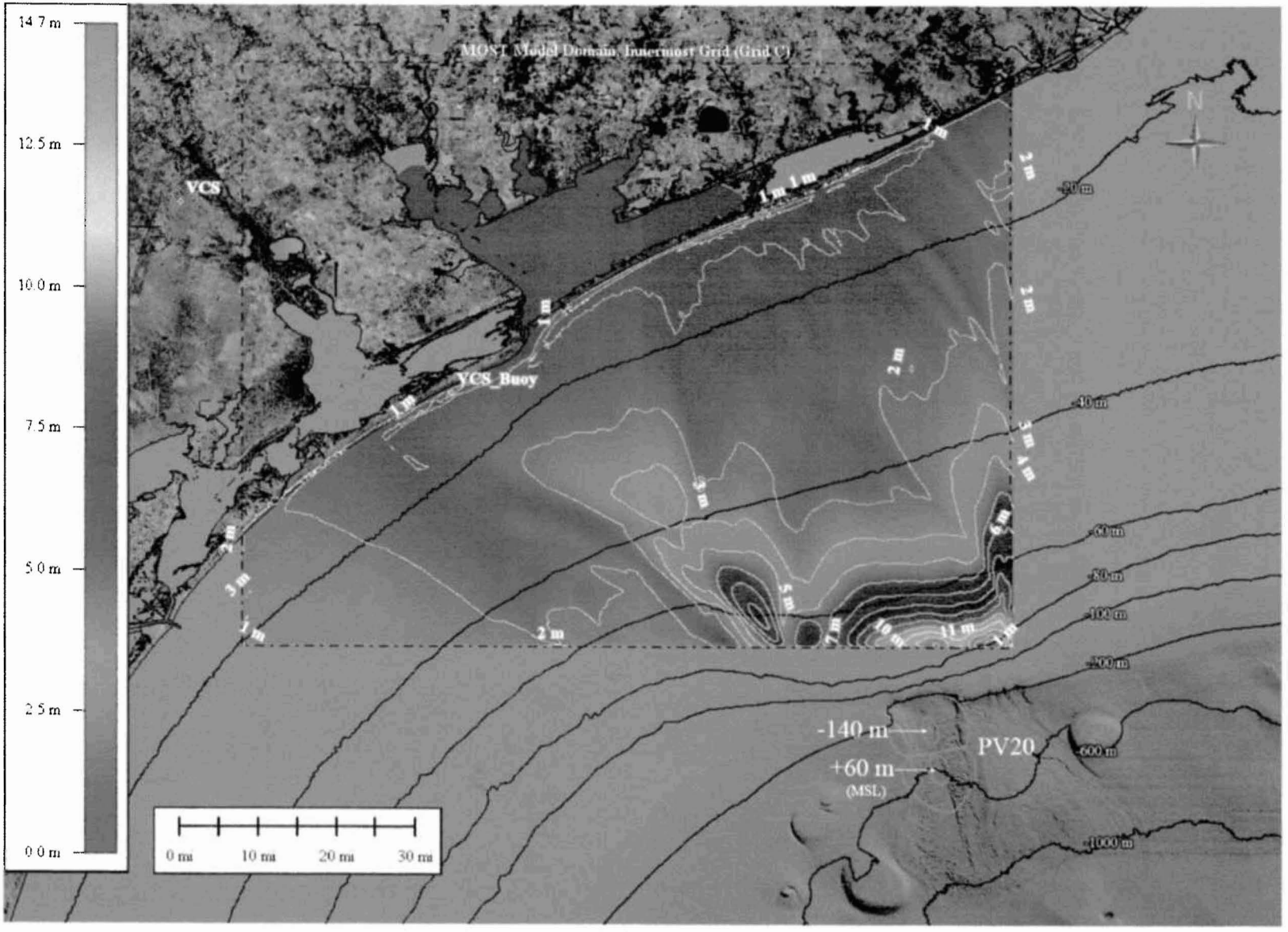

Figure 2.4.6-11 Maximum water surface elevations (MSL) for simulation case PV20. Maximum tsunami runup elevation: 2 m (MSL), with negligible inundation past the barrier islands. Bathymetry elevations are relative to MSL.

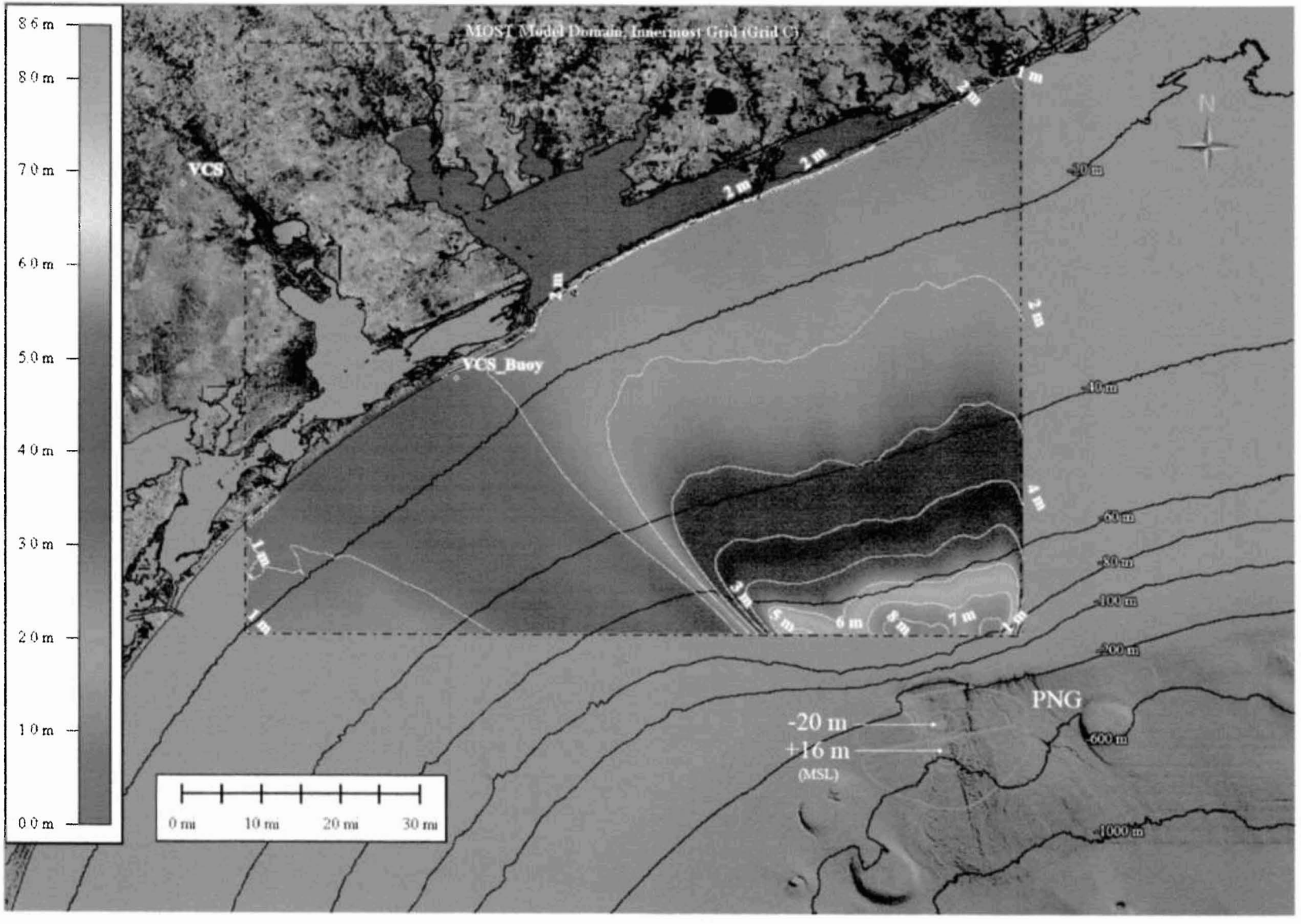

Figure 2.4.6-12 Maximum water surface elevations (MSL) for simulation case PNG. Maximum tsunami runup elevation: 2 m (MSL), with negligible inundation past the barrier islands. Bathymetry elevations are relative to MSL.

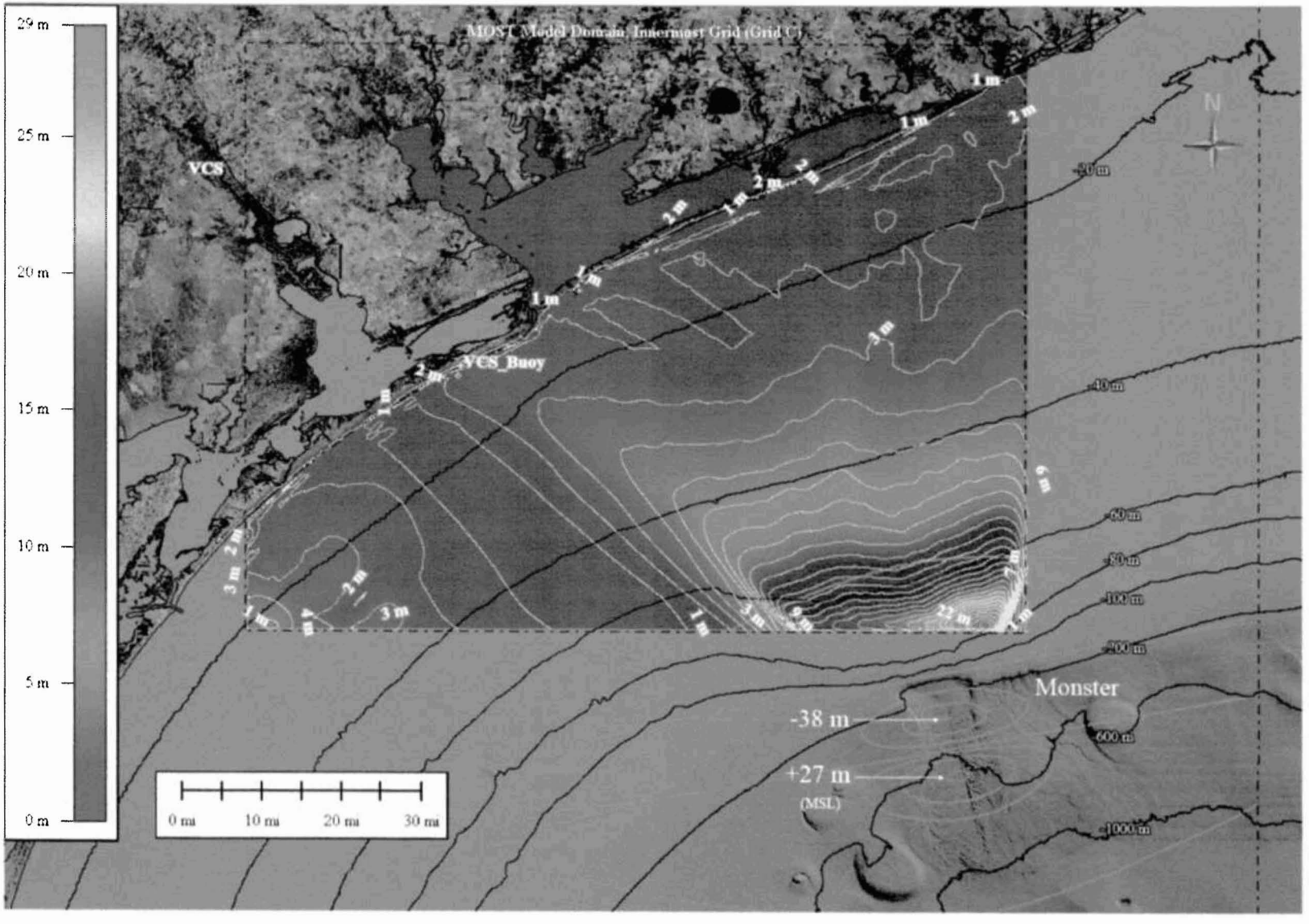

Figure 2.4.6-13 Maximum water surface elevations (MSL) for simulation case "Monster." Maximum tsunami runup elevation: 2 m (MSL), with negligible inundation past the barrier islands. Bathymetry elevations are relative to MSL.

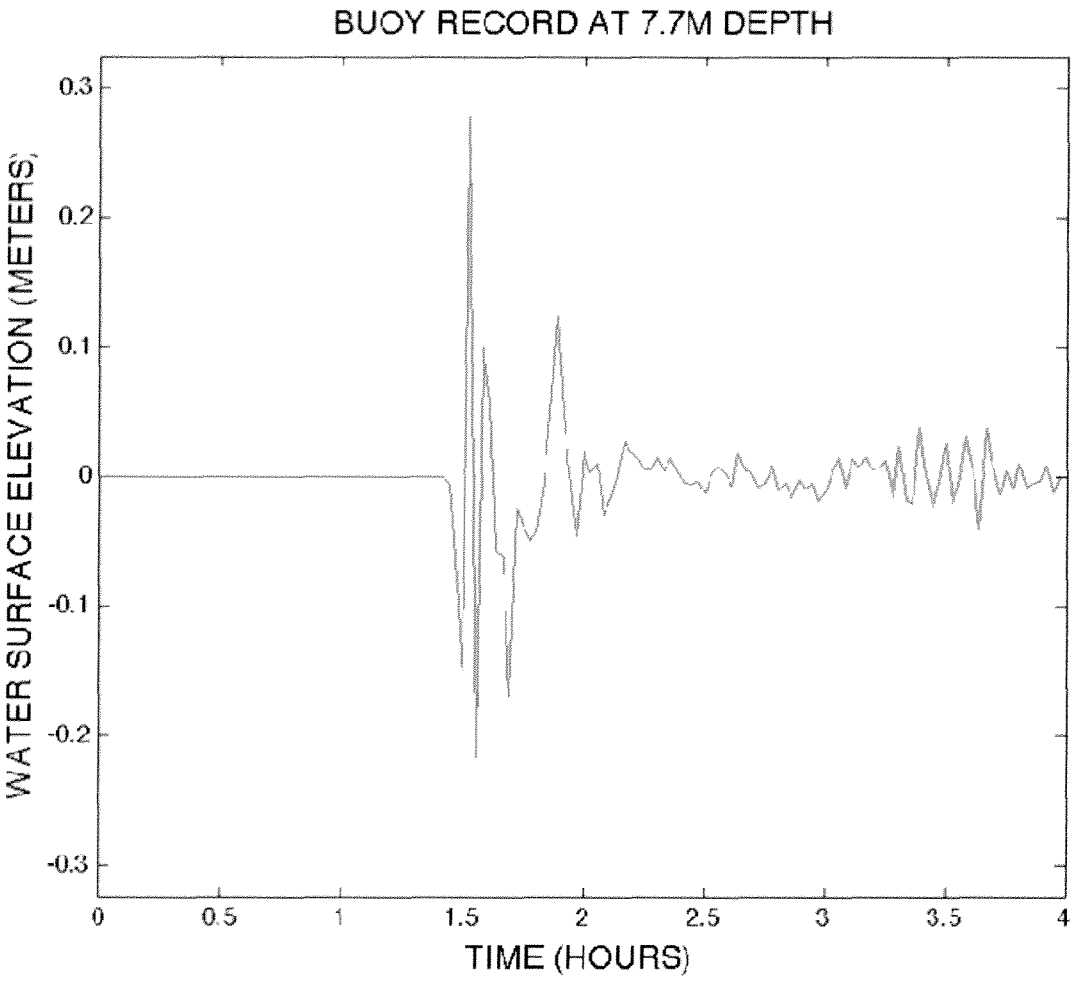

Figure 2.4.6-14 Water surface elevation (MSL) time record for a hypothetical buoy for simulation case PV at a latitude of 28.2633° N and longitude of 96.532° W (VCS_Buoy in Figure 2.4.6-8).

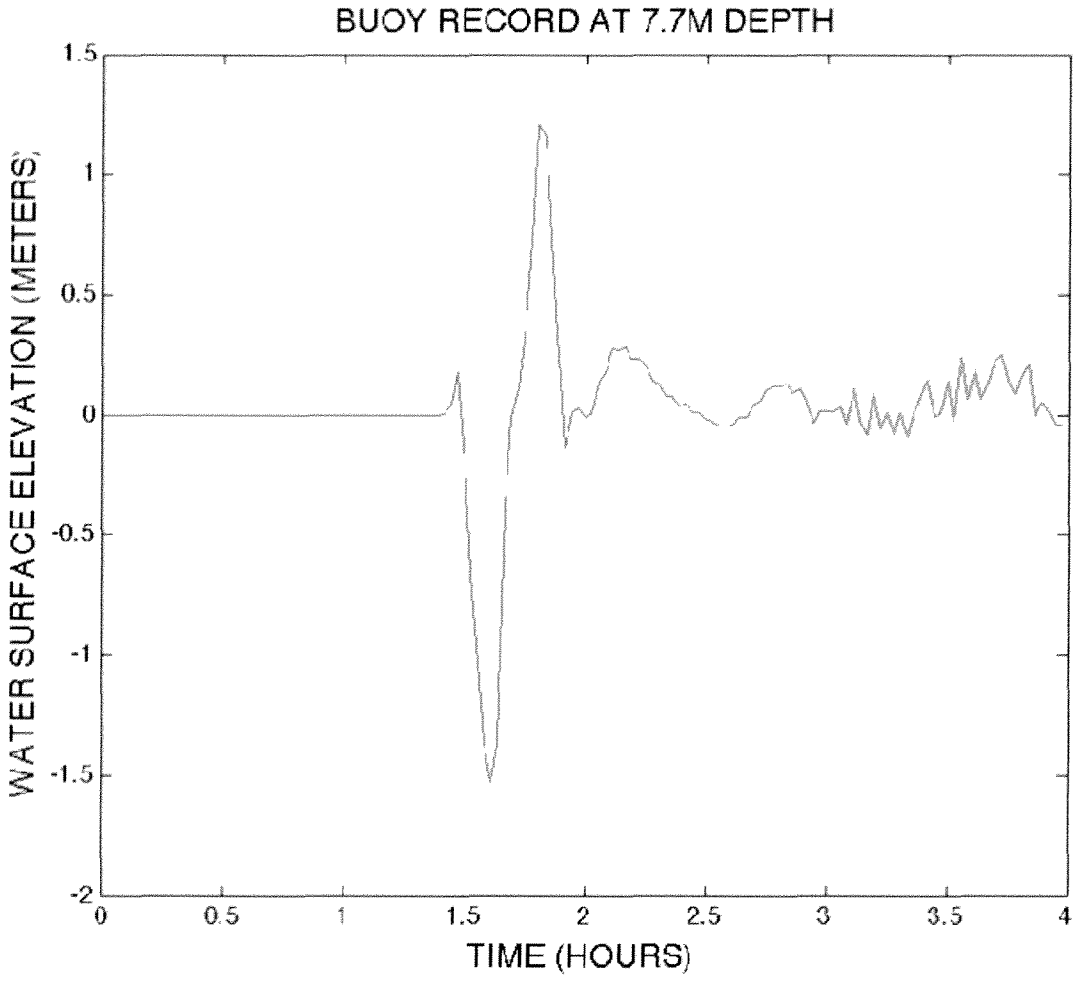

Figure 2.4.6-15 Water surface elevation (MSL) time record for a hypothetical buoy for simulation case PV20 at a latitude of 28.2633° N and longitude of 96.532° W (VCS_Buoy in Figure 2.4.6-8).

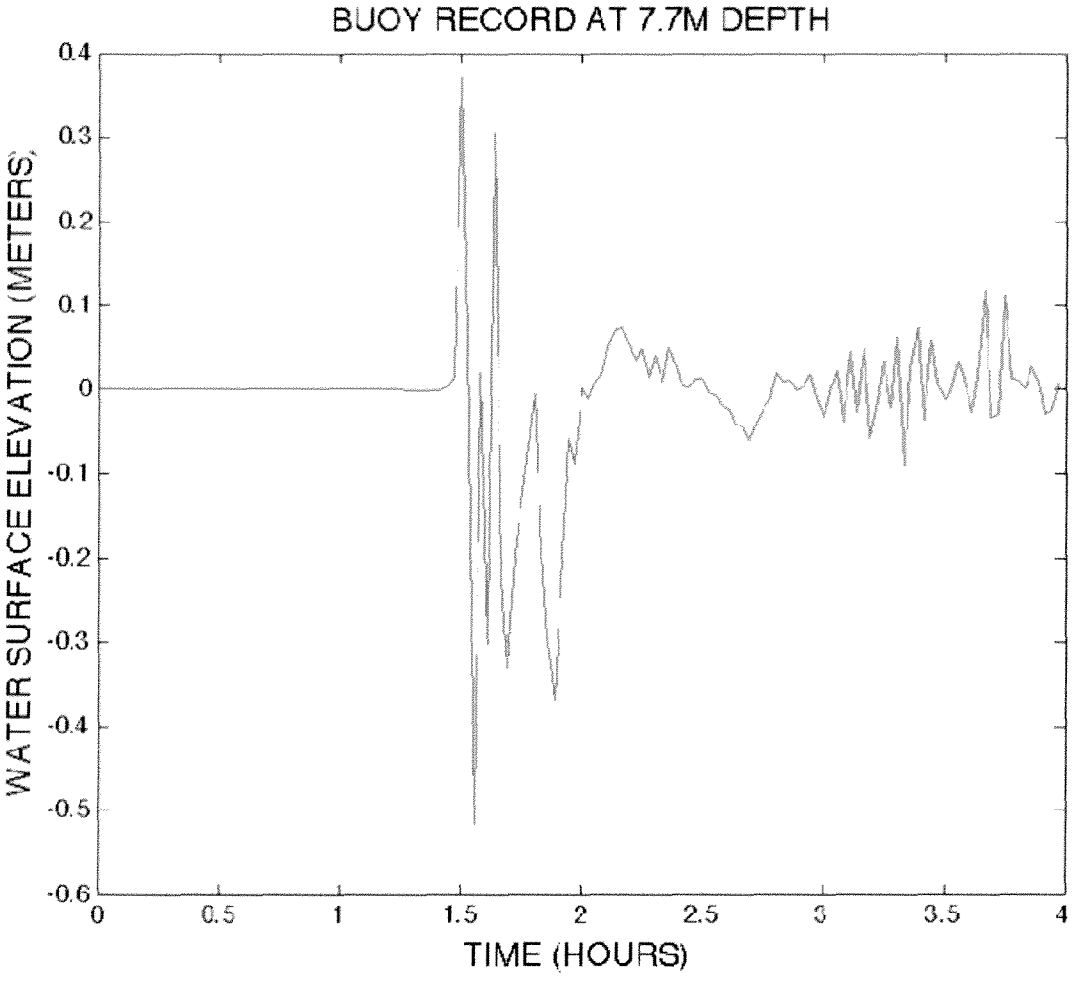

Figure 2.4.6-16 Water surface elevation (MSL) time record for a hypothetical buoy for simulation case PNG at a latitude of 28.2633° N and longitude of 96.532° W (VCS_Buoy in Figure 2.4.6-8).

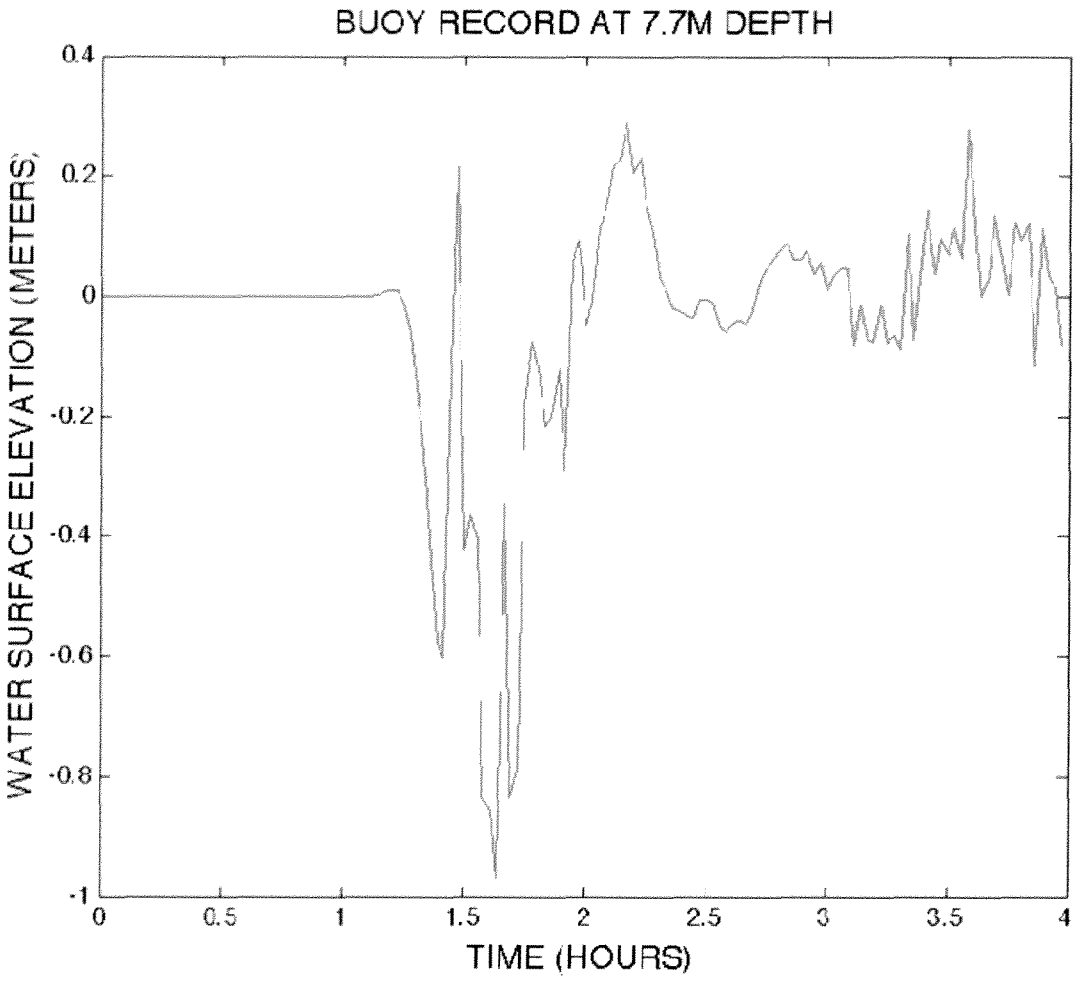

Figure 2.4.6-17 Water surface elevation (MSL) time record for a hypothetical buoy for simulation case "Monster" at a latitude of 28.2633° N and longitude of 96.532° W (VCS_Buoy in Figure 2.4.6-8).

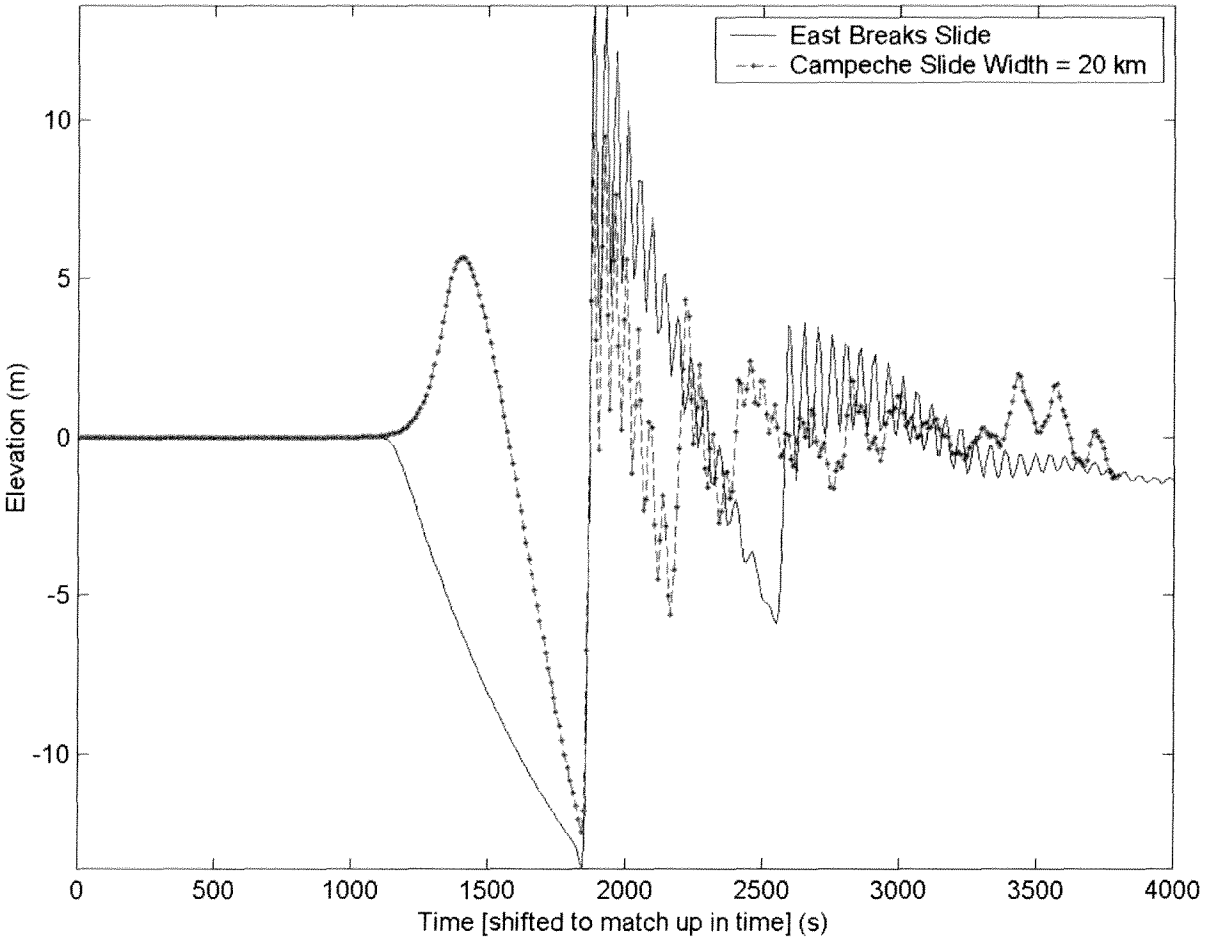

Figure 2.4.6-18 Synthetic tsunami time series (marigrams) for the Campeche hypothetical landslide scenario and East Breaks landslide scenario. Water surface elevations relative to MSL. Ocean water depth assumed to be 50 m (Source: Reference 2.4.6-18).

RAI 02.05.02-10:

Question:

In SSAR Section 2.5.2, the applicant characterizes seismic hazard for the VCS site. In accordance with 10 CFR 100.23, the staff requests the applicant provide additional information regarding its seismic hazard characterization.

SSAR Figure 2.5.1-51 shows locations of oil and gas wells in southern Victoria County. Oil and gas exploration and extraction are capable of inducing seismic events. In SSAR Section 2.5.2, the applicant did not discuss human-induced seismicity resulting from gas and oil extraction. Please discuss the history of any induced seismicity from oil and gas extraction in the region and the future potential for increased seismic hazard at the VCS site.

Response:

Seismicity associated with oil and gas production-activities commonly is related to: (1) hydraulic fracturing, (2) oil and gas extraction, or (3) injection of waste water or other fluids for enhanced recovery (Davis et al., 1995; Davis et al., 1989).

Hydraulic fracturing is a method of injecting high-pressure fluids with sand into relatively massive and unfaulted rocks to fracture the rock and thus create pathways for the extraction of oil and gas (Davis et al., 1989; Frohlich and Davis, 2002). The dimensions of hydraulic fractures depend on numerous factors (e.g., volume of fluid and sand injected, the permeability of the formation, and the variation of the minimum horizontal stress over depth), but in general the longest dimension of an individual fracture is no more than hundreds to thousands of feet (Coulter et al., 2004; Fisher et al., 2004; Gale et al., 2007). Therefore, induced seismicity from hydraulic fracturing is expected to be below levels normally detected by regional seismic networks (Modified Mercalli Intensity I or less) and thus of no danger to surface structures (Albright and Pearson, 1980; Majer et al., 2007; Maxwell et al., 2006).

Small magnitude earthquakes (mb less than about 5) can be induced by fluid extraction (e.g., Davis et al., 1989; Frohlich and Davis, 2002; Segall, 1989) or fluid injection (e.g., Majer et al., 2007; Majer and Peterson, 2007; Seeber et al., 2004). Fluid extraction is generally thought to induce seismicity through poroelastic changes in the in situ stress state (e.g., Segall, 1989; Van Eijs et al., 2006). Several earthquakes within south-central Texas have been attributed to local oil and gas extraction. The largest of these earthquakes is the 9 April 1993 mbLg 4.3 event (Davis et al., 1995) that occurred over 60 miles to the west of the VCS site (Figure 1) and is mentioned in RAI 02.05.02-1.

Fluid injection is thought to trigger seismicity by reducing the effective stress across faults (through increasing the pore pressures) and thus weakening the faults (Frohlich and Davis, 2002; Majer et al., 2007). The largest earthquake associated with fluid injection reported in Texas is the 16 June 1978 mb 4.3 to 4.6 earthquake near Snyder, over 350 miles to the northwest of the VCS site (Figure 1) (Davis and Pennington, 1989; Frohlich and Davis, 2002). This event was part of a series of earthquakes associated with fluid injection within the Cogdell oil field. Beginning in later 2008, a series of small earthquakes with mb $\leq$ 3.3 have occurred near the Dallas-Fort Worth airport, over 290

miles from the VCS site (Figure 1). Despite the small magnitudes of these earthquakes, they have received extensive media coverage due to their association with waste water injection (Frohlich et al., 2011; Frohlich et al., 2010).

SSAR Figure 2.5.2-2 shows the seismicity surrounding the site as well as the 200-mile (site region) and 50-mile buffers around the site. As shown in SSAR Figure 2.5.2-2, there is no seismicity within 50 miles of the site and relatively little seismicity within 200 miles of the site. The seismicity shown in this figure comprises earthquake epicenters in both the original EPRI-SOG seismicity catalog and the updated seismicity catalog developed for the VCS site (see SSAR Section 2.5.2.1). As described in SSAR section 2.5.2.1 and in the response to RAI 02.05.02-1, the updated catalog includes tectonic earthquakes and has had all likely man-made earthquakes removed. The response to RAI 02.05.02-1 briefly discusses four man-made earthquakes that have been removed from the updated catalog. Three of these events (July 1991, April 1993, May 1993) are the closest reported man-made earthquakes to the VCS site with Emb ≥ 3.0. The closest approach of these earthquakes to the site is approximately 60 miles (Figure 1). Therefore, there are no reported man-made earthquakes, including any earthquakes triggered by oil and gas production-related activities (e.g., extraction, injection, hydraulic fracturing) within 50 miles of the site. Given the absence of earthquakes associated with oil and gas production within 50 miles of the site, despite the presence of oil and gas wells surrounding the site (SSAR Figure 2.5.1-52), and the small magnitudes of earthquakes related to oil and gas production within Texas, earthquakes associated with oil and gas production are not likely to increase the seismic hazard for the VCS site.

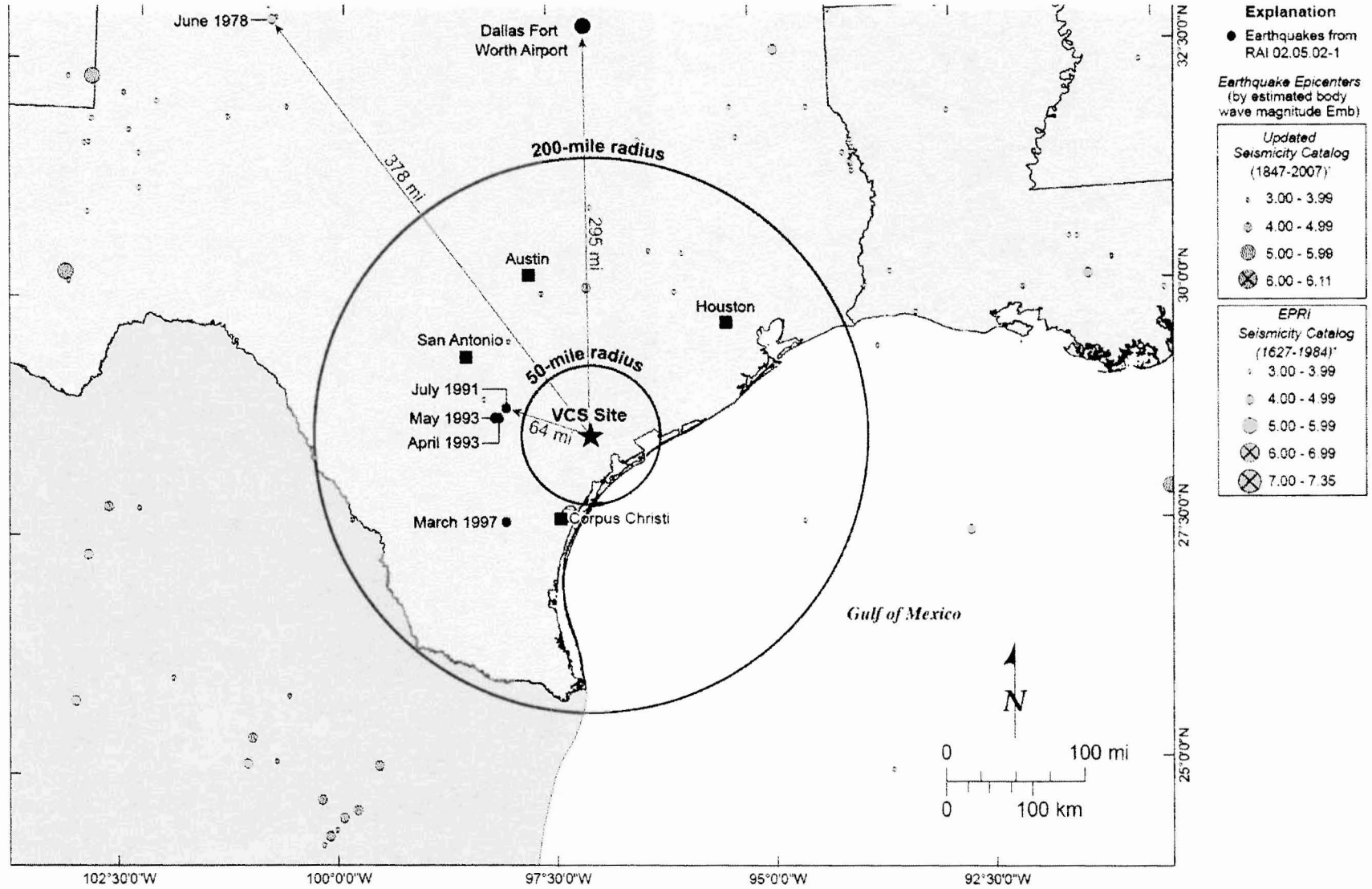
June 1978
Dallas Fort Worth Airport
378 mi
295 mi
200-mile radius
50-mile radius
Austin
Houston
San Antonio
July 1991
May 1993
April 1993
VCS Site
64 mi
March 1997
Corpus Christi
Gulf of Mexico
N
0
100 mi
0
100 km
102°30'0"W
100°0'0"W
97°30'0"W
95°0'0"W
92°30'0"W
32°30'0"N
30°0'0"N
27°30'0"N
25°0'0"N
Explanation
Earthquakes from RAI 02.05.02-1
Earthquake Epicenters (by estimated body wave magnitude Emb)
Updated Seismicity Catalog (1847-2007)
3.00 - 3.99
4.00 - 4.99
5.00 - 5.99
6.00 - 6.11
EPRI Seismicity Catalog (1627-1984)
3.00 - 3.99
4.00 - 4.99
5.00 - 5.99
6.00 - 6.99
7.00 - 7.35

Figure 1.

References:

Albright, J., and Pearson, C., 1980, Location of hydraulic fractures using microseismic techniques, Society of Petroleum Engineers of AIME annual technical conference and exhibition, Volume SPE-9509: Dallas, TX

Coulter, G.R., Benton, E.G., and Thomas, C.L., 2004, Water Fracs and Sand Quantity: A Barnett Shale Example, SPE Annual Technical Conference and Exhibition: Houston, TX, Society of Petroleum Engineers, Inc.

Davis, S.D., Nyffenegger, P.A., and Frohlich, C., 1995, The 9 April 1993 earthquake in South-Central Texas: Was it induced by fluid withdrawal?: Bulletin of the Seismological Society of America, v. 85, p. 1888–1895.

Davis, S.D., and Pennington, W.D., 1989, Induced seismic deformation in the Cogdell oil field of west Texas Bulletin of Seismological Society of America, v. 79, p. 1477-1495.

Davis, S.D., Pennington, W.D., and Carlson, S.M., 1989, A compendium of earthquake activity in Texas, University of Texas at Austin, Bureau of Economic Geology, Geological Circular 89-3

Fisher, M.K., Heinze, J.R., Harris, C.D., Davidson, B.M., Wright, C.A., and Dunn, K.P., 2004, Optimizing horizontal completion techniques in the Barnett Shale using microseismic fracture mapping, Society of Petroleum Engineers Annual Technical Conference: Houston, TX, Society of Petroleum Engineers

Frohlich, C., and Davis, S.D., 2002, Texas Earthquakes: Austin, University of Texas Press, 275 p.

Frohlich, C., Hayward, C., Stump, B., and Potter, E., 2011, The Dallas–Fort Worth Earthquake Sequence: October 2008 through May 2009: Bulletin of Seismological Society of America, v. 101, p. 327-340.

Frohlich, C., Potter, E., Hayward, C., and Stump, B., 2010, Dallas-Fort Worth earthquakes coincident with activity associated with natural gas production: Leading Edge, v. 29, p. 270-275.

Gale, J.F.W., Reed, R.M., and Holder, J., 2007, Natural fractures in the Barnett Shale and their importance for hydraulic fracture treatments: AAPG Bulletin, v. 91, p. 603–622.

Majer, E.L., Baria, R., Stark, M., Oates, S., Bommer, J., Smith, B., and Asanuma, H., 2007, Induced seismicity associated with Enhanced Geothermal Systems: Geothermics, v. 36, p. 185-222.

Majer, E.L., and Peterson, J.E., 2007, The impact of injection on seismicity at The Geysers, California Geothermal Field International Journal of Rock Mechanics and Mining Sciences, v. 44, p. 1079–1090.

Maxwell, S.C., Waltman, C.K., Warpinski, N.R., Mayerhofer, M.J., and Boroumand, N., 2006, Imaging Seismic Deformation Induced by Hydraulic Fracture Complexity, Society of Petroleum Engineers Annual Technical Conference and Exhibition, September 2006, San Antonio, Texas, paper SPE-102801.

Seeber, L., Armbruster, J.G., and Kim, W.-Y., 2004, A Fluid-Injection-Triggered Earthquake Sequence in Ashtabula, Ohio: Implications for Seismogenesis in Stable Continental Regions Bulletin of Seismological Society of America, v. 94, p. 76-87.

Segall, P., 1989, Earthquakes triggered by fluid extraction: Geology, v. 17, p. 942-946.

Van Eijs, R.M.H.E., Mulders, F.M.M., Nepveu, M., Kenter, C.J., and Scheffers, B.C., 2006, Correlation between hydrocarbon reservoir properties and induced seismicity in the Netherlands: Engineering Geology, v. 84, p. 99-111.

Associated ESPA Revisions:

The following will be added to a new subsection in a future revision of the SSAR.

2.5.2.1.6 Seismicity Associated with Petroleum Production Activities

The updated seismicity catalog was developed for the VCS site to exclude man-made earthquakes (e.g., those related to oil and gas production). Earthquakes related to oil and gas production can be caused by hydraulic fracturing and/or fluid extraction and injection (e.g., oil and gas withdraw, wastewater injection). Earthquakes associated with hydraulic fracturing generally produce ground motions well below normally detectable levels (i.e., MMI I or less) (Albright and Pearson, 1980; Majer et al., 2007; Maxwell et al., 2006). Within Texas, earthquakes with magnitudes greater than mb 3.0 that are associated with fluid injection and extraction are rare and all have magnitudes less than mb 5.0 (Reference 2.5.2-4) (Davis et al., 1989). The closest reported earthquakes with magnitudes greater than mb 3.0 to the VCS site are a series of earthquakes near the town of Flashing that occurred in 1991 and 1993 over 60 miles to the west of the VCS site. These earthquakes are not in the updated catalog developed for the VCS site because they are man-made events. The largest man-made earthquake, associated with oil and gas extraction, was a magnitude mbLg 4.3, occurred on 9 April 1993 that occurred over 60 miles (97 km) to the west of the VCS site (Davis et al., 1995). Given the absence of earthquakes associated with oil and gas production near the VCS site, and the small magnitudes of earthquakes related to oil and gas production, these types of earthquakes are not likely to have a significant impact on the seismic hazard of the VCS site.

ATTACHMENT 3

SUMMARY OF REGULATORY COMMITMENTS

(Exelon Letter to USNRC, NP-11-0028, dated June 30, 2011)

The following table identifies commitments made in this document. (Any other actions discussed in the submittal represent intended or planned actions. They are described to the NRC for the NRC's information and are not regulatory commitments.)

COMMITMENT	COMMITTED DATE	COMMITMENT TYPE	
		ONE-TIME ACTION (Yes/No)	Programmatic (Yes/No)
Exelon will revise the VCS ESPA SSAR Section 2.4.6 to incorporate the change shown in the enclosed response to the following NRC RAI: 02.04.06-3 (Attachment 1)	Revision 1 of the ESPA SSAR and ER planned for no later than March 31, 2012	Yes	No
Exelon will revise the VCS ESPA SSAR Section 2.5.2 to incorporate the change shown in the enclosed response to the following NRC RAI: 02.05.02-10 (Attachment 2)	Revision 1 of the ESPA SSAR and ER planned for no later than March 31, 2012	Yes	No